Model Studies on the Phase Behavior of 4-cyano-4'-n-pentyloxybiphenyl: Molecular Dynamics Simulations

Vom Fachbereich Chemie
der Technischen Universität Darmstadt

zur Erlangung des akademischen Grades eines

Doctor rerum naturalium (Dr. rer. nat.)

genehmigte
Dissertation

vorgelegt von

M. Sc. Chem. Saniye Pinar Sargin

aus Ankara

Berichterstatter:	Prof. Dr. J. Brickmann
Mitberichterstatter:	Prof. Dr. W. Haase

Tag der Einreichung: 16. Dezember 1999
Tag der mündlichen Prüfung: 31. Januar 2000

Darmstadt 2000

Meinem Freund Bastiaan Robert Wegewijs

Die vorliegende Arbeit wurde im Fachbereich Chemie, Fachgebiet Physikalische Chemie I, auf Anregung und unter Anleitung von Herrn Prof. Dr. J. Brickmann in der Zeit von Juni 1995 bis Dezember 1999 durchgeführt.

Mein Dank gilt an dieser Stelle

Herrn Prof. Dr. J. Brickmann für die interessante Themenstellung, die stetige Unterstützung und die mir gewährte Entfaltungsfreiheit,

den Herren Dr.-Ing. H.J. Bär und Dr.-Ing. S.M. Kast für zahlreiche interessante und anregende Diskussionen,

den Herren Dr.-Ing. K. Nicklas, Dipl.-Ing. M. Müller und Dipl.-Physico-Chimiste S. Longatte für ihre Unterstützung in technischen Fragen,

den Herren Dipl.-Ing. T.E. Exner, Dipl.-Ing. F. Schmidt und Dipl.-Phys. D. Zahn für ihre freundliche Hilfestellung bei der Übersetzung ins Deutsche,

den Herren Dipl.-Phys. T. Gunkel, Dr.-Ing. U. Schmitt, Dipl.-Ing. H. Merx und Dipl.-Ing. R. Jäger,

allen Mitgliedern des Arbeitskreises für die freundschaftliche Atmosphäre,

sowie der Volkswagenstiftung und dem Deutschen Akademischen Austausch Dienst für die finanzielle Förderung.

TABLE OF CONTENTS

CHAPTER I

INTRODUCTION

The term liquid crystal signifies a state of aggregation that is intermediate between the crystalline solid and the amorphous liquid [1-3]. A substance in this state is strongly anisotropic in some of its properties and yet shows a certain degree of fluidity, which in some cases is comparable to that of an ordinary liquid. The first observations of liquid crystalline or *mesomorphic* behavior were made towards the end of the last century by Reinitzer [4] and Lehmann [5]. An essential requirement for mesomorphism to occur is that the molecule must be highly anisotropic. The system may pass through one or more mesophases before it is transformed into the isotropic liquid. Transitions to these intermediate states may be brought about by purely thermal processes (*thermotropic* mesomorphism) or by the influence of the solvent (*lyotropic* mesomorphism).

Thermotropic liquid crystals (the nomenclature was originally proposed by Friedel [6]) are classified broadly into three types: *nematic*, *cholesteric* and *smectic*. The names *nematic* and *smectic* liquid crystals come from the Greek word for thread and for soap respectively. The nematic liquid crystal has a high degree of long range orientational order of the molecules, but no long range translational order. Consequently, it differs from the isotropic liquid in that the

molecules are spontaneously oriented with their long axes approximately parallel. Nematic liquid crystals can be formed by molecules that have a more or less elongated shape. The cholesteric mesophase is also a nematic type of liquid crystal except that it is composed of optically active molecules. In the smectic liquid crystal, the system can be viewed as a set of two-dimensional liquid layers stacked on each other with a well defined spacing.

Liquid crystalline systems have attracted considerable scientific interest in the past 20 years, not only because of their wide technical applications like liquid crystal displays (LCD) for watches, calculators, telephones etc., but also because of their important role towards a fundamental understanding of how molecules behave cooperatively and how molecular structure influences this behavior.

Liquid crystalline behavior is determined by molecular properties such as shape, flexibility, charge distribution and polarizability. Theoretical studies of the liquid crystalline behavior have a long history going back to Onsager [7]. The early well-known work of Maier and Saupe has been widely used to describe many properties of liquid crystals [8-11]. This theory is based on the description of the liquid crystalline molecule as a rigid rod which interacts with a mean field created by the surrounding molecules. Contributions of the alkyl chain as a flexible extension were first considered by Marcelja [12]. Although these theories may explain many liquid crystalline properties, they are unable to relate the observed phase behavior to the detailed structural characteristics and molecular properties.

Compounds like 4-cyano-4'-*n*-alkyloxybiphenyl (nOCB), 4-cyano-4'-*n*-alkylbiphenyl (nCB), where *n* stands for the number of carbon atoms in the alkyloxy (or in the alkyl) group, are known to be rod-shaped molecules, which have an elongated, anisotropic geometry allowing for preferential alignment along one spatial direction [13]. They are of broad research interest for investigations on pure phases as well as on solutions. Moreover, they are used in commercial mixtures for LCD applications [14]. Crystal and the molecular structure of some of them (nOCB with n=1,2,3,4, nCB with n=2,3,5) have been examined by Haase and coworkers [15-18]. Besides the experimental interest, the field of liquid crystals has also attracted a large number of computational investigations. Various simulations have been performed, which used a full atom representation for liquid crystalline materials within molecular dynamics (MD) and Monte Carlo (MC) techniques [19-29]. However, realistic modeling of materials such as 5OCB [19,20,22], 5CB [23] is quite expensive considering the limits of today's computer power. Hence less complex models have been used in the MD and MC computer simulations, which consider the effect of some of the above mentioned molecular properties on the liquid crystalline behavior [30-36].

The aim of this work is to examine the influence of the force field parameters on the isotropic and the liquid crystalline phase behavior of the model system for 5OCB (Fig. 1) by means of MD simulation. The 5OCB molecule has the phase sequences crystal–nematic–isotropic: Cr. 321 N 341 I (in K) [37]. The phase behavior investigation of the 5OCB molecule by MD simulations using the full atom calculations is restricted to short simulation times due to the

expensiveness of the computation time [19, 20,22]. Hence, in the present work a series of simplifications have been carried out on the model system to investigate the phase behavior of the 5OCB molecule. The representation of the phenyl ring as a *sphere*, formed by a united atom [36], the inclusion or the exclusion of the electrostatic interactions, and the treatment of the 5OCB molecule as a semi-flexible model or as a rigid-body model are the main simplifications carried out in this work. Those simplifications allow a longer simulation time while analyzing the dynamical properties as well as the structural properties of both the isotropic and the liquid crystalline phases for 5OCB as a function of temperature and the density; such as the diffusion coefficient, the orientational order parameter, and the radial, angular, and time correlation functions. Furthermore, the results of the MD simulations are compared to those of the full atom calculations of the same system[19,20,22] and to the available experimental data like orientational order parameter, density, and the self-diffusion coefficient [37-41].

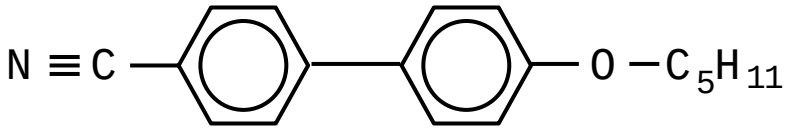

Figure 1 Structure of 5OCB.

CHAPTER II

COMPUTATIONAL ASPECTS

The motivations for applying computer simulation techniques to study microscopic systems of chemical and physical interest are manifold. Computer simulations open a pathway to extract numerically exact results for problems in statistical mechanics which would otherwise only be soluble within an approximate framework. In this sense, computer simulation can be regarded as a test of theories. The simulations results may also be compared to those of real experiments, which is a way to test the validity of model assumption invoked in the simulation. Thus, computer simulations play a dual role as a bridge, on the one hand between models and theoretical predictions, and on the other hand, between models and experimental results. Owing to this connecting role and the way in which simulations are conducted and analyzed, computer simulations are therefore often called *numerical experiments*.

Computer simulations provide information about the macroscopic properties of experimental interest (the equation of state, transport coefficients, structural order parameters etc.) from the microscopic details of a system (the masses of the atoms, the interaction between atoms, molecular geometry and so on). Moreover, simulations can partly substitute experiments when experiments cannot resolve certain microscopic aspects of interest, such as the detailed microscopic reaction mechanism etc..

Simulation methods are nowadays an established tool in many branches of science. The dramatic development of computer power as well as the enormous algorithmic improvements have given rise to a significantly increased interest in studying complex systems consisting of more than 10^4 atoms using molecular dynamics (MD) technique; one of the main type of simulation methods applied [42].

2.1 Statistical Ensembles

An "*ensemble*" is the assembly of all possible microstates- all states consistent with the constraints with which one can characterize system macroscopically. The common ensembles treated in MD simulations are the microcanonical (constant-NVE), the canonical (constant-NVT) and the isothermal-isobaric (constant-NpT) ensemble. For each ensemble, the thermodynamic variables defined in brackets are fixed. For instance, the assembly of all microstates with fixed energy E, volume V and particle number N is called a microcanonical ensemble, or that of with fixed particle number N, pressure p, and temperature T is called isothermal-isobaric ensemble, and so on.[42].

2.2 The Molecular Dynamics Simulation Technique

Classical MD simulations are based on the numerical solution of Newton's equations of motion of a many-body system

$$m_i \ddot{\mathbf{r}}_i(t) = \mathbf{F}_i(t) = -\nabla_i V_{tot} \tag{1}$$

$$\mathbf{p}_i(t) = m_i \dot{\mathbf{r}}_i(t) \tag{2}$$

where **r** denotes the Cartesian position vector of particle *i*, **F** the force acting on that particle, *m* its mass, *V* the potential and **p** the momentum. The solution yields phase space trajectories of an ensemble resembling the collection of points in phase space. If the forces can be derived from a potential field, which is independent of time and velocities (as in Eqn. 1), the total energy is a constant of motion. Analytical solutions to Eqn. (1) and (2) can be found only for a limited number of idealized systems such as the free particle and coupled harmonic oscillators.

The integration procedures are based on a *discretization* of the continuous time *t* into *N* discrete time steps $\ddot{a}t$. For large systems (up to 10^5 particles), the numerical strategies have to be optimized in order to keep the numerical effort within acceptable limits.

The most widely used method of integrating the equations of motion was initially proposed by Verlet [43]. The Verlet integrator shows for a given time step Δt comparatively small numerical errors for conserved quantities, and it involves only one force calculation per step. The Verlet method is a direct

solution of the second-order equations (see Eqn. 1) and it is based on positions **r***(t)*, forces **F***(t)* and positions from the previous step:

$$\mathbf{r}(t+\Delta t) = 2\mathbf{r}(t) - \mathbf{r}(t-\Delta t) + \Delta t^2 \frac{\mathbf{F}_i(t)}{m_i} \quad . \tag{3}$$

The velocities are needed for determining the kinetic energy, and thus the total energy. They may be obtained from the formula

$$\mathbf{v}(t) = \frac{\mathbf{r}(t+\Delta t) - \mathbf{r}(t-\Delta t)}{2\Delta t} \tag{4}$$

In the Verlet algorithm, the positions are correct up to an error of the order of Δt^4 while the velocities are correct up to an order of Δt^2. Nonetheless, this integration method gives even with long time steps better energy conservation than other integration methods [44,45]. This stems from the sympletic properties of the discrete mapping in phase space, which are preserved within the Verlet algorithm. Furthermore, the algorithm is time-reversible and symplectic.

The main numerical effort of an MD simulation is related to the calculation of long range interactions (Coulombic and Lennard-Jones interactions). If the interactions between all particles are included, the computational expense is proportional to the square of the particle number N as far as only pair potentials are employed. Since the common intermolecular potential approaches zero for large distances it is advisable to calculate the interaction energy and the forces within a limited region around a given site only in order to reduce the numerical effort.

The truncation of the intermolecular potential at a certain spherical cutoff distance r_{cut} introduces some difficulties in defining a consistent potential and force for use in the MD method. It is the function of the shifted force (SF) potentials to modify the truncated potential in such a way that both the potential and force decay to zero when approaching r_{cut}. Furthermore, the cutoff distance should not be greater than ½ of the box length L for consistency with the minimum image convention. In this work, the CHARMM cutoff potential [46] for Coulomb and LJ interactions is used and the periodic boundary conditions are applied so that the number density in the system is conserved.

2.2.1 MD Simulations of Constant-NVT and Constant-NpT Ensembles

Simulations in the canonical (NVT) ensemble, i.e., at a constant temperature require that the equations of motion of a simulated system are coupled to an external heat bath. The heat bath introduces the energy fluctuations which are necessary to keep a fixed temperature and generates states in the canonical ensemble.

In the applied MD program, the stochastic thermalization method developed by Kast et al. [47] is used as a constant temperature algorithm. The method is based on collisions between system particles and fictitious heat bath particles of finite mass.

MD simulations at constant pressure are helpful to equilibrate systems where the initial configuration is far from equilibrium and are necessary to

calculate observables within the NPT ensemble. In this work, the technique developed by Berendsen et al. is applied [48]. This technique adjusts the density of the system to a given pressure. At each time step, the volume of the box is scaled by a factor of μ, and the molecular center-of-mass coordinates are scaled by a factor of $\mu^{1/3}$:

$$\mathbf{r}' = \mu^{1/3}\mathbf{r} \tag{5}$$

with

$$\mu = 1 - \frac{\kappa \Delta t}{3\beta_p}\left(P_o - P\right) \tag{6}$$

where κ stands for the coupling constant, μ is the scaling factor, Δt is the simulation time step, P_o is the desired pressure, and β_p is the compressibility. This algorithm lets the system reach equilibrium irrespective of possible restrictions caused by a fixed volume or by the shape of the simulation box.

2.2.2. Constraint Dynamics

Constraint dynamics algorithms are a helpful tool in MD calculations of systems where a fully rigid or partially rigid description of molecules is appropriate. Following a classical mechanics description, atoms are modeled by point particles interacting according to the prescribed potential energy, which is conveniently divided into an intramolecular and intermolecular part. When the intramolecular potential is a sum of continous contributions, the molecule is said

to be *flexible*. If the interactions between some groups of atoms in the molecule are fixed by geometrical constraints, the molecule is then *partly rigid*. When all intramolecular interactions are modeled by geometrical constraints, the molecule is *fully rigid*. The essential motivation to apply constraints rests on the purpose to eliminate the fast vibrational modes, thus allowing a larger time step to be used in the simulations in order to decrease the numerical expense.

In the applied MD program, two types of constraint dynamics algorithms are used, namely Ciccotti's algorithm [49] for simulations of the rigid part of the molecular model and the SHAKE [50] algorithm, for elimination of the bond stretching motions to keep the bond distances constant.

2.3. Quantities Obtained from MD Simulations

2.3.1 Order Parameter

The liquid crystalline state is characterized by the existence of long-range orientational order. Nematic phases can be described by a single order parameter defining the preference of the molecules to align in one direction, i.e. along the axis of preferred orientation (director). The degree of alignment is described by the *nematic orde*r parameter, that is the average of the 2nd order Legendre polynomial [51]:

$$S = \left\langle P_2(\cos \hat{a}) \right\rangle = \frac{3}{2}\left\langle \cos^2 \hat{a}_i \right\rangle - \frac{1}{2}. \qquad (7)$$

In the original theory [52], as well as in much of the literature, the symbol *S* is used to represent the *nematic order* parameter $\langle P_2(\cos\hat{a})\rangle$. In a computer simulation this order parameter could in principle be evaluated using :

$$S = \frac{1}{N_{tot}} \sum_{i=1}^{N_{tot}} \left(\frac{3}{2} \left\langle \cos^2 \hat{a}_i \right\rangle - \frac{1}{2} \right) \tag{8}$$

with

$$\cos\hat{a}_i = \vec{\mathbf{n}} \cdot \vec{\mathbf{u}}_i \text{, and } \vec{\mathbf{u}}_i = (x_i, y_i, z_i). \tag{9}$$

Here, $\hat{a}_i$ is the angle between the long axis of the molecule *i* represented by a unit vector $\vec{\mathbf{u}}_i$ (composed of three components x_i, y_i, and z_i) and the director $\vec{\mathbf{n}}$, N_{tot} is the total number of molecules, and the brackets denote the ensemble average. In a system where the axes are perfectly aligned with respect to the director, *S* equals to 1. The order parameter *S* becomes zero when the molecular axes are randomly distributed like in the isotropic phase. In the *nematic* phase, *S* has an intermediate value which is temperature dependent. In practice, however, the orientation of the nematic director is not known a priori. Thus, *S* cannot be calculated according to Eq(8). For the large number of molecules, $\vec{\mathbf{n}}$ can be estimated by

$$\vec{\mathbf{n}} \approx \frac{1}{N_{tot}} \sum_i \vec{\mathbf{u}}_i \,. \tag{10}$$

Nevertheless, the most accurate way of determining the orientation of the nematic director is to calculate *S* from the ordering tensor $\hat{\mathbf{Q}}$:

$$S' = \frac{1}{N_{tot}} \left\langle \sum_{i=1}^{N_{tot}} \left(\frac{3}{2} (\vec{\mathbf{n}} \cdot \vec{\mathbf{u}}_i)^2 - \frac{1}{2} \right) \right\rangle$$

$$= \frac{1}{N_{tot}} \frac{3}{2} \sum_{i=1}^{N_{tot}} \left\langle \vec{\mathbf{n}}. \left(\vec{\mathbf{u}}_i \vec{\mathbf{u}}_i - \frac{1}{3} \hat{\mathbf{I}} \right) . \vec{\mathbf{n}} \right\rangle$$

where $\hat{\mathbf{I}}$ is the identity matrix and, thus, the ordering tensor $\hat{\mathbf{Q}}$ can be expressed as :

$$\hat{\mathbf{Q}} = \frac{3}{2} \sum_{i}^{N_{tot}} \begin{bmatrix} x_i x_i - \frac{1}{3} & x_i y_i & x_i z_i \\ y_i x_i & y_i y_i - \frac{1}{3} & y_i z_i \\ z_i x_i & z_i y_i & z_i z_i - \frac{1}{3} \end{bmatrix}. \qquad (11)$$

Then the order parameter takes the bilinear form :

$$S' = \frac{1}{N_{tot}} \sum_{i=1}^{N_{tot}} \left\langle \vec{\mathbf{n}} \,.\, \hat{\mathbf{Q}} \,.\, \vec{\mathbf{n}} \right\rangle . \qquad (12)$$

The diagonalization of $\hat{\mathbf{Q}}$ gives the three eigenvalues $\ddot{e}_+ , \ddot{e}_o , \ddot{e}_-$. One can define the *nematic order* parameter *S* as the largest eigenvalue ($\ddot{e}_+$) of $\hat{\mathbf{Q}}$, while the corresponding eigenvector defines the director $\vec{\mathbf{n}}$ [53].

2.3.2 Time Correlation Functions

Time correlation functions measure to what extent the value of some dynamical quantity *A(t)* at time *t* is related to the value of some other quantity *B(*t′*)* at time t'. If *A(t)* and *B*(t') represent two time-dependent signals, the time correlation function is defined by

$$C(t)=\langle A(t_o)\,B(t')\rangle$$

with $t=t'-t_o$

(13)

The ensemble average of the Eq. (13) can be written as a time average

$$C(t)=lim\frac{1}{\ddot{e}}\int_{o}^{\ddot{e}_{max}} A(\ddot{e}+t_o)\,B(\ddot{e}+t')\,d\ddot{e}. \qquad (14)$$

The function *C(t)* measures the correlation between the value of *A* at time t_o and that of *B* at time t'. When *A* and *B* are the same quantity, *C* is called an *auto correlation* function and then *C* measures how the value of *A* at t' is correlated with its value at t_o:

$$C(t)=\langle A(t_o)\,A(t')\rangle\ . \qquad (15)$$

The quantity *A(*t_o*)* is expressed as a function of particle positions and velocities. In this work, the first type of autocorrelation function is calculated (see

Eg. 16). If $A(t_o)$ is defined, e.g as the particle positions as a function of time, then the non-normalized C(t) looks like

$$C(t) = C_{\mathbf{uu}} = \frac{1}{N_{tot}} \sum_{i=1}^{N_{tot}} \left\langle \vec{\mathbf{u}}_i(t_o)\, \vec{\mathbf{u}}_i(t_o + t) \right\rangle_{t_o}, (A \equiv \mathbf{u}). \quad (16)$$

where $\vec{\mathbf{u}}_i$ is the vector specifying the orientation of the molecule *i*, and N_{tot} is the total number of molecules in the system.

2.3.3 The Diffusion Coefficient

The molecular self-diffusion coefficients, which are important observables to quantify the molecular mobility, are calculated by invoking the Einstein relation [42], in which the diffusion coefficient D is related to the mean square displacement (MSD) by

$$2\, D\,(t - t_o) = \frac{1}{3} \left\langle \left[\mathbf{r}_i(t) - \mathbf{r}_i(t_o)\right]^2 \right\rangle . \quad (17)$$

Here $\mathbf{r}_i(t)$ is the position of a molecular center of mass at the simulation time t. Similarly, one can write the self-diffusion coefficient along the x-direction D_x,(and analogous expressions for D_y and D_z) as:

$$D_x\,(t - t_o) = \frac{1}{2} \left\langle \left[\mathbf{x}_i(t) - \mathbf{x}_i(t_o)\right]^2 \right\rangle \quad (18)$$

2.3.4 Radial Pair Distribution Function *g(r)*

In the condensed phase, the microscopic structure can be characterized by a set of pair distribution functions for the atomic positions. The simplest of them is the radial pair distribution function *g(r)*. This function is a measure for the number of atoms within a sphere of radius r and is characterized by the expression *g(r)* :

$$g(r) = \frac{V_{tot}}{N_{tot}} \frac{1}{M} \left\langle \sum_{i=1}^{M} \frac{dn_i(r)}{4\delta r^2 dr} \right\rangle \tag{19}$$

where V_{tot} is the volume of the system, N_{tot} the total number of molecules in the system, M the number of shells of width dr, and $dn_i(r)$ is the number of molecules between r and $r + dr$.

2.3.5 Cylindrical Pair Distribution Functions *g(z,R)*

A more detailed insight into the orientation of the molecules can be obtained from pair distribution functions in cylindrical coordinates. The cylindrical pair distribution function *g(z,R)* is defined by

$$g(z,R) = \frac{V_{tot}}{N_{tot}} \frac{1}{M} \left\langle \sum_{i=o}^{M} \frac{dn_i(z,R)}{2\delta R\, dR\, dz} \right\rangle \tag{20}$$

where z is the coordinate along the cylinder axis, R is the distance perpendicular to this coordinate, dz the length of the cylinder disk and $dn_i\ (z,R)$ the number of molecules in the space limited by R and $R+dr$ and by z and $z+dz$.

CHAPTER III

MODEL DESCRIPTION

3.1 Isotropic State

Two models have been set up for 5OCB (see Figure 1), termed SF/M1 (semi-flexible M1) and SF/M2 (semi-flexible M2). The numbering of the atoms in 5OCB for both models is depicted in Fig. 2.

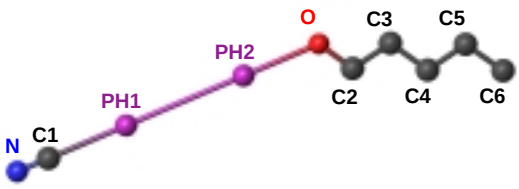

Figure 2 Numbering of the atoms in 5OCB

The general features of the models are:

(1). The fragment of the molecule between nitrogen (N) and oxygen (O) is kept rigid (see Fig. 2).

(2). Each methylene group in the alkyl chain is represented as a *united atom*, which allows to treat the CH group as a single interaction center. This approach greatly reduces the total number of atoms in the system, which results in considerable reduction in computer time. In order to achieve a realistic description of the alkyl chain, the valence angles formed by three methylene groups and the torsional angles of four neighboring united atoms in the alkyl chain remain flexible.

(3). The intramolecular bond lengths are constrained in both models (see Table 1).

(4). The C-C bond lengths in the alkyl chain are fixed at a distance of 1.55 Å (see Table 1).

(5). A combination of the SHAKE algorithm [50] and the method of Ciccotti et al. [49] is applied in order to constrain the intramolecular bond lengths and the rigid parts of the molecule.

(6). The interaction potential function is expressed by

$$V = V_{NB} + V_{Valence} + V_{Torsion} \tag{21}$$

where V_{NB} represents the nonbonded interactions, $V_{Valence}$ and $V_{Torsion}$ are the contributions from the valence angles $\grave{e}_{ijk}$ and the dihedral angles $\ddot{o}_{ijkl}$ respectively:

$$V_{Valence} = \sum_{i,j,k} \frac{1}{2} k_{Valence} \left(\grave{e}_{ijk} - \grave{e}_{ijk,o} \right)^2 \tag{21a}$$

$$V_{Torsion} = \sum_{i,j,k,l} \sum_{1}^{4} H_n \left[1 - cos\left(n\ddot{o}_{ijkl}\right)\right] \qquad (21b)$$

Interactions between force centers that are separated by more than three bonds are defined by nonbonded potentials. These nonbonded interactions consist of a Coulomb and a Lennard-Jones (LJ) term :

$$V_{NB}(r_{ij}) = \frac{1}{4\delta\mathring{a}_0} \frac{q_i q_j}{r_{ij}} + 4\mathring{a}_{ij} \left[\left(\frac{\acute{o}_{st}}{r_{ij}} \right)^{12} - \left(\frac{\acute{o}_{st}}{r_{ij}} \right)^{6} \right] \qquad (22)$$

(7). The phenyl rings are treated as a *sphere*, formed by a *united atom* [36]. In order to have a simplicity in terms of comparing the results with the full atom calculations, i.e. to compare the effect of the simple model on the calculations, the force field parameters were taken from the work by Hauptmann [19] except those for the nonbonded parameters of the phenyl rings. The latter were parameterized to obtain the experimental density according to Ref. 54. All force field parameters used in this work for the nonbonded interactions, valence angles and torsional potentials are listed in Table 2, 3 and Table 4 respectively.

The main difference between SF/M1 and SF/M2 is that in SF/M1 all charges are set to zero; the Coulomb interaction is completely neglected. In contrast, in SF/M2 charges are included on the atoms of the rigid part of the molecule as well as on the C2 atom of the flexible part (see Table 2 and Fig. 2). The charges for PH1 and PH2 were obtained by summation of the charges on the phenyl rings of the full atom calculations [19].

3.2 Nematic State

In the isotropic state no pronounced difference is observed between the SF/M1 and the SF/M2 model. Hence, the SF/M1 model, where the electrostatic interactions are excluded, was not used in the liquid crystalline state. In addition to the SF/M2 model of the isotropic state, one more model has been used for the nematic state of 5OCB; namely the rigid body model (RB/M2). The RB/M2 model is a modification of the SF/M2 model. The interaction potential definition is the only quantity which distinguishes the RB/M2 model from the SF/M2 one. In contrast to SF/M2, the interaction potential of RB/M2 is composed of only non-bonded interactions ($V = V_{NB}$, see Eqn.22). In other words, the contributions of the valence angles and the dihedral angles of the SF/M2 model are omitted in the RB/M2 model so that each molecule is treated as a rigid body. The bond lengths, charges and the non-bonded parameters in the RB/M2 model are defined as being similar to that of the SF/M2 model (see Table 1 and Table 2).

Figure 3 summarizes the models used in the isotropic and the nematic phase.

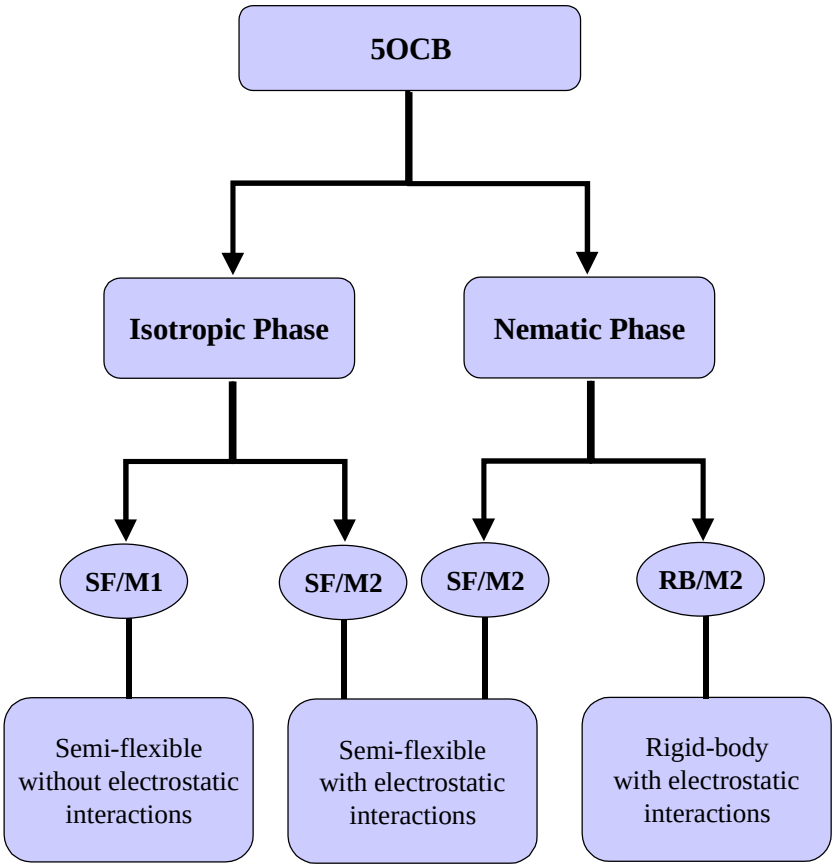

Figure 3 A schematical representation of the models used in the isotropic and the nematic state.

Table 1 Bond lengths used in the semi-flexible SF/M1, SF/M2, and the rigid body RB/M2 model.

	SF/M1-M2, RB/M2
Bond Type	Bond length ( )
C1-N	1.13
C1-PH1	2.84
PH1-PH2	4.32
PH2-O	2.76
O-C2	1.44
C2-C3	1.55
C3-C4	1.55
C4-C5	1.55
C5-C6	1.55

Table 2 The non-bonded parameters and the atomic charges used in the semi-flexible SF/M1,SF/M2, and the rigid body RB/M2 model.

	SF/M1	SF/M2,RB/M2	SF/M1-M2,RB/M2	SF/M1-M2,RB/M2
Atom Type	Charge	Charge	σ [ ]	[kJ/mol]
N	0	0.430	3.200	0.711
C1	0	0.395	3.649	0.628
PH1	0	-0.055	4.100	5.420
PH2	0	0.225	4.100	5.420
O	0	-0.385	3.000	0.711
C2	0	0.250	3.906	0.494
C3-C5	0	0	3.906	0.494
C6	0	0	3.906	0.732

Table 3 Force field parameters for the valence angle potential used in the semi-flexible SF/M1 and the SF/M2 model

	SF/M1-M2	SF/M1-M2
Bond angle	K_θ (kJ/rad^2)	θ_0 (rad)
PH2-O-C2	836.780	111.800
O-C2-C3	669.425	109.500
C2-C3-C4	527.172	112.400
C3-C4-C5	527.172	112.400
C4-C5-C6	527.172	112.400

Table 4 Force field parameters for the torsional potential used in the semi-flexible SF/M1 and the SF/M2 model

	SF/M1-M2	SF/M1-M2	SF/M1-M2	SF/M1-M2
Torsion	H1 (kJ/mol)	H2 (kJ/mol)	H3 (kJ/mol)	H4 (kJ/mol)
PH2-O-C2-C3	0.000	0.000	0.000	0.000
O-C2-C3-C4	1.130	0.000	-8.368	0.000
C2-C3-C4-C5	6.278	3.348	-5.859	0.000
C3-C4-C5-C6	7.115	2.930	-6.278	0.000

CHAPTER IV

RESULTS AND DISCUSSION

4.1 Isotropic State

4.1.1 Computational Details

All MD simulations have been performed in a rectangular box with periodic boundary conditions containing 144 molecules that are randomly orientated at the start of the simulation. The initial configuration is generated at a fairly low density in order to ensure that the molecules are separated far enough from each other to avoid any overlap. Starting from this low density configuration, the system is first compressed until a reasonable density is reached. This volume reduction is achieved by decreasing the box size by a fixed percentage μ (see Table 5) along each direction of the box at every time step. To adjust the size of the simulation box after each compression step, the NpT [48] simulation technique was applied at T = 400 K and p = 1 bar with a pressure coupling constant of $\hat{a}$ = 0.002 Pa s. All trajectories are integrated using the Verlet algorithm [43] with a discrete time steps of 2 fs. The density obtained during the NpT simulation is 0.998 g/cm^3 and 1.02 g/cm^3 for model SF/M1 and SF/M2 respectively. The experimental density for 5OCB at 349 K is 1.02 g/cm^3

[40] The lower value of SF/M1 owes to the fact that the electrostatic interactions in SF/M1 are excluded.

After reaching an equilibrium distribution, where the average of the box volume, potential and kinetic energy remain constant, MD simulations in the NVT ensemble [47] for a total simulation time of 1000 ps are carried out in order to analyze the phase properties.

In all simulations shifted potentials [46] with a cutoff radius of 13 Å for the nonbonded interaction are used. In Table 5 and 6, the parameters used in the applied NpT and NVT simulations are listed.

Table 5 Parameters applied in the NpT simulations of the SF/M1 and the SF/M2 model in the isotropic state at 400 K.

Total number of molecules	144
Temperature	400 K
Thermostat coupling constant	0.001
Pressure coupling constant β	0.002 Pa s
Pressure P_o	1 bar
Simulation time step Δt	2 fs
Compression factor μ	$1*10^{-4}$
Cut-off Radius r_{cut}	13 Å

Table 6 Parameters applied in the NVT simulations of the SF/M1 and the SF/M2 model in the isotropic state at 400 K.

Temperature	400 K
Thermostat coupling constant	0.001
Volume	63684 $Å^3$
Simulation time	1000 ps

4.1.2 Dynamical Properties

The self-diffusion coefficients of SF/M1 and SF/M2 over a total simulation time of 1000 ps are summarized in Table 7. All values in Table 7 are obtained by NVT simulations at 400 K. One can see that the D_{tot} value of SF/M1 is $9.98*10^{-6}$ cm^2s^{-1} while the calculated value for the SF/M2 case is found to be $4.82*10^{-6}cm^2s^{-1}$. This is a direct consequence of the inclusion of the electrostatic interactions in the model SF/M2, resulting in a decrease of the molecular mobility. The same kind of trend is also observed comparing the self-diffusion coefficients D_x, D_y , D_z of model SF/M1 and that of model SF/M2 (see Table 7). Furthermore, the SF/M2 results show pronounced differences between D_x, D_y and D_z values. It is known that the self-diffusion coefficients in the isotropic phase are larger than 10^{-6} cm^2 s^{-1} [26]. Although all diffusion coefficients for SF/M2 are greater than 10^{-6} cm^2 s^{-1} , the differences between D_x, D_y and D_z values might still be attributed to the anisotropy of the system. In that case, the system in SF/M2 probably

resembles a "*glass*" like state. In contrast to this, the results of the full atom calculations (see Table 7), where all partial charges on the nuclei are included, do not show significant differences between D_x, D_y and D_z values [19].

Table 7. Self-diffusion coefficient of 5OCB from mean square displacements (MSD) over a total simulation time of 1000 ps compared with those of the full atom calculations [19] (simulation time 239 ps). All values are the results of the NVT simulations in the isotropic state at 400 K

	SF/M1	SF/M2	Full Atom [Ref. 19]
D_{tot}	$9.98*10^{-6}$	$4.82*10^{-6}$	$2.8*10^{-6}$
D_x	$9.82*10^{-6}$	$3.62*10^{-6}$	$3.1*10^{-6}$
D_y	$1.01*10^{-5}$	$6.04.*10^{-6}$	$2.7*10^{-6}$
D_z	$9.99*10^{-6}$	$4.79*10^{-6}$	$2.4*10^{-6}$

In order to extract the differences in the dynamical behavior of model SF/M1 and SF/M2, the normalized time correlation function *C(t)* for the rigid core (N-O) and for the flexible alkyl chain (C2-C6) is calculated as a function of time according to Eqn. (16). By definition, *C(t)* is a real-valued function ranging from 0 to 1. Values close to 1 indicate a high degree of similarity or correlation. Fig. 4a shows the time correlation function of the alkyl chain (from C2 to C6) for model SF/M1 and SF/M2, while Fig. 4b exhibits *C(t)* only for the rigid part of the molecule (from N to O). Both figures show that there is a significant decorrelation

on the time scale of 1000 ps. It is seen that the decorrelation time of SF/M2 in both Fig. 4a and Fig. 4b is longer than that of the SF/M1 model. The difference in the correlation time in Fig. 4b is more pronounced than in Fig. 4a. Additionally, the longer decorrelation time of both SF/M1 and SF/M2 as seen in Fig. 4b is reasonable because of the imposed rigidity of selected bonds of the molecule (the N-O bond). For a liquid system, the *C(t)* function takes the negative values as well. The absence of the negative values in both graphs shows again that the system resembles a kind of a "*glass*" like state.

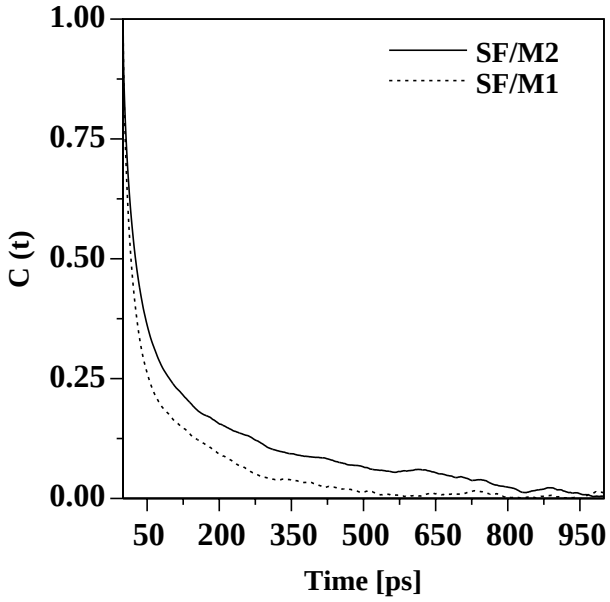

Figure 4a. The normalized time correlation function for the alkyl chain (C2-C6) in the isotropic state at 400 K.

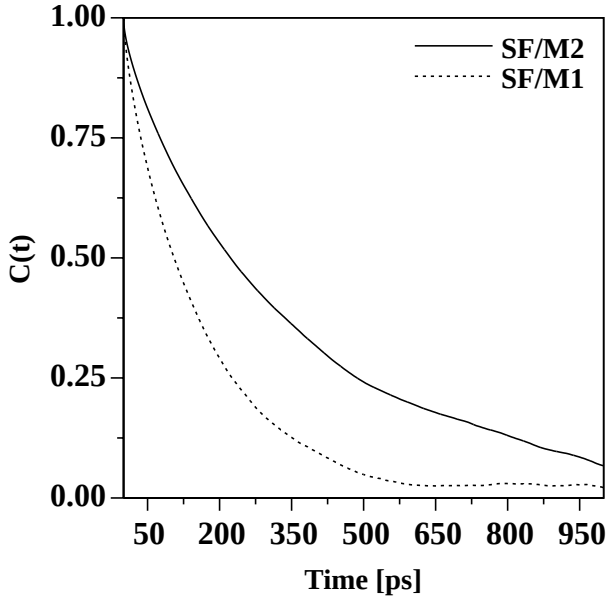

Figure 4b. The normalized time correlation function for the rigid part of the molecule (N-O) in the isotropic state at 400 K.

4.1.3 Structural Properties

In order to study the orientation of the molecules with respect to a director, the order parameter *S* is calculated according to the method of Eppenga and Frenkel [53] (see section 2.3.1).

In the isotropic phase, where the molecular axes are randomly distributed, the order parameter *S* is zero. Table 8 displays the order parameter averaged over all configurations of the simulations at 400 K. Since the fragment of the molecule from N to O is rigid, the same values for *S* are observed for this part of the molecule in both models. Furthermore, all values of *S* are close to zero for both SF/M1 and SF/M2, showing that at 400 K the molecules prefer a random orientation. It can also be seen that the inclusion of the electrostatic interactions

has no major effect on the orientational order manifested in the order parameters. Ono and Kondo carried out a molecular dynamics calculation for 5OCB in the nematic and the isotropic state by using realistic atom-atom interaction potentials with the NVT simulation technique. Their calculations on the orientational order parameter in the isotropic state at 360 K revealed that $S = 0.24$ [20], which is quite surprising in terms of observing some order in the isotropic state. In the calculations of the present work, however, S is found to be $3.40*10^{-2}$ for SF/M1 and $5.05*10^{-2}$ for SF/M2, which shows the random orientation of the 5OCB molecules in both SF/M1 and SF/M2 model at 400 K.

Table 8. Order parameters (*S*) averaged over all configurations as a result of the NVT simulations in the isotropic state at 400 K.

	S (SF/M1)	*S* (SF/M2)
N – C1	$3.53*10^{-2}$	$5.87*10^{-2}$
C1 - PH1	$3.53*10^{-2}$	$5.87*10^{-2}$
PH1 –PH2	$3.53*10^{-2}$	$5.87*10^{-2}$
PH2 –O	$3.53*10^{-2}$	$5.87*10^{-2}$
N – O	$3.53*10^{-2}$	$5.87*10^{-2}$
C2 - C4	$9.08*10^{-3}$	$1.28*10^{-2}$
C4 - C6	$4.73*10^{-3}$	$1.25*10^{-2}$
C3 - C5	$1.06*10^{-2}$	$1.11*10^{-2}$
C2 - C6	$1.01*10^{-2}$	$1.15*10^{-2}$
N – C6	$3.40*10^{-2}$	$5.05*10^{-2}$

Another way to examine the molecular orientation is to compute the angular distribution, which is defined by means of the angle between the longest molecular axis and the director. In the present work, the longest molecular axis coincides with the z axis.

Figure 5a illustrates the distribution function of the phenyl rings (PH1-PH2) for model SF/M1 and SF/M2 in addition to the theoretical angle distribution function in the isotropic phase, which is :

$$P(\grave{e}) = \frac{1}{2} sin(\grave{e}) \qquad (23)$$

It is seen that the inclusion of the electrostatic interactions on the rigid part of the 5OCB molecule leads to a partial order, while the exclusion of them leads to the ideal uniform distribution.

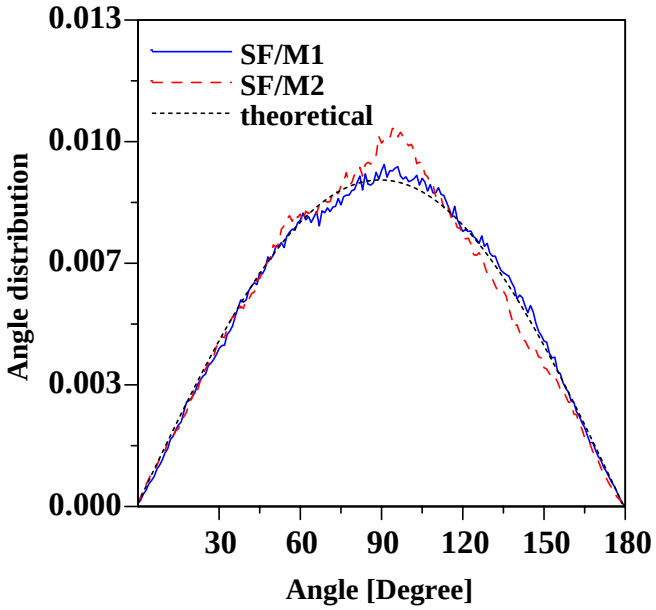

Figure 5a. Angular distribution function of the phenyl rings (PH1-PH2) and the theoretical angular distribution function in the isotropic phase .

In Figure 5b, where the angular distribution function of the alkyl chain (C4-C6) is plotted, the maximum value for both model SF/M1 and SF/M2 is

located at 90°. In other words, the inclusion of the electrostatic interactions does not change the molecular orientation concerning the flexible alkyl chain.

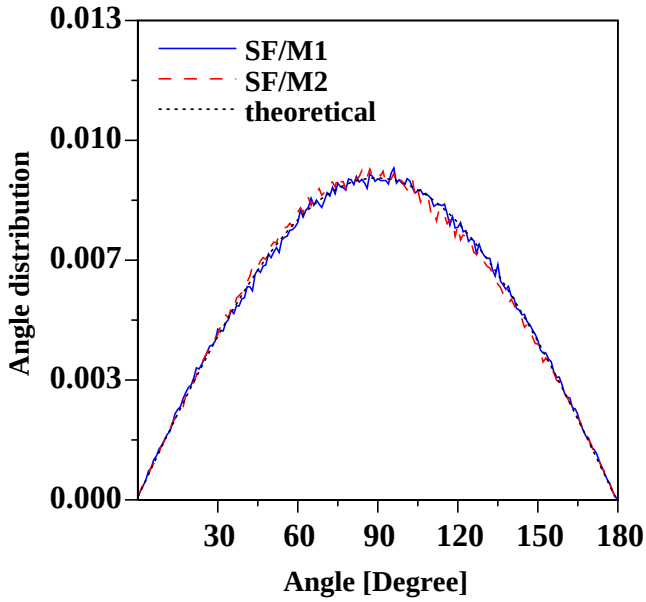

Figure 5b. Angular distribution function of the alkyl chain (C4-C6) and the theoretical angular distribution in the isotropic phase.

The radial pair distribution function for the nitrogen-nitrogen atom pairs of SF/M1 and SF/M2 is displayed in the top part of Fig. 6a. The first maximum represents the nearest neighbors in the first coordination shell. In contrast to SF/M1 model, where only van der Waals interactions are considered, there is a dominated second shell in the SF/M2 model where the electrostatic interactions are included.

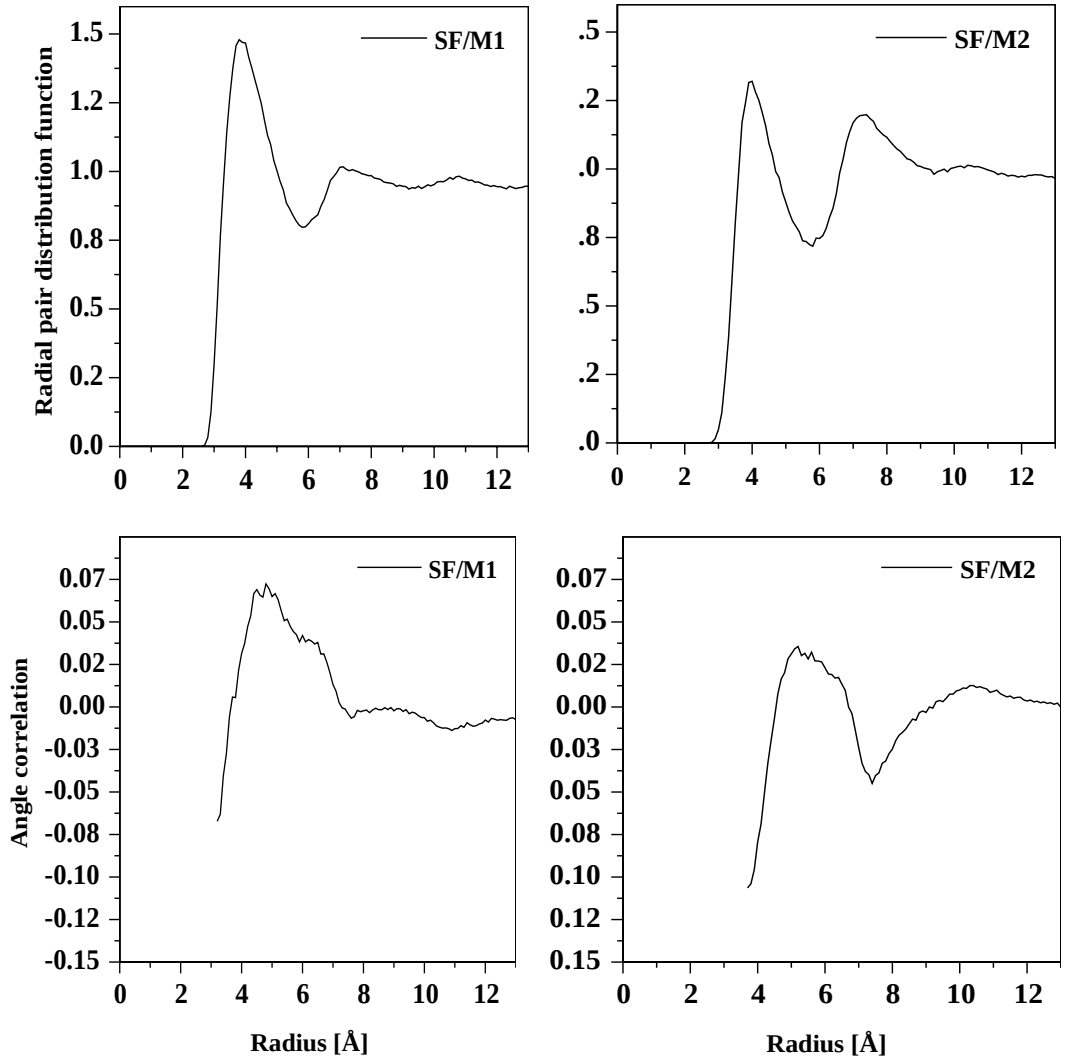

Figure 6a. Radial pair distribution function *g(r)* of the nitrogen atoms (top) and angle correlation function $P_{uu}(r)$ for the angle between two cyano groups (bottom) from the NVT simulation in the isotropic state at 400 K

Orientational correlation functions are another method of examining the local structure of the isotropic state. The relative orientation of the two neighboring cyano groups can be described by the angle ρ between the two bond vectors. The dependence of this angle on the distance between the two nitrogen atoms can be discussed in terms of the angle correlation function $P_{uu}(r)$

$$P_{uu}(r) = \left\langle \cos \tilde{n}_{ij} \right\rangle_r = \left\langle \mathbf{u}_i \mathbf{u}_j \right\rangle_r \qquad (24)$$

where **u** is a unit vector in the direction from the nitrogen atom to the carbon atom of the cyano group. The negative values of $P_{uu}(r)$ stem from the antiparallel orientation of the molecules while positive values of $P_{uu}(r)$ results from a parallel orientation of the molecules.

The exclusion of the electrostatic interactions strengths the parallel orientation of the neighboring CN group at small N-N distances in the isotropic state. The $P_{uu}(r)$ of SF/M2 , similar to SF/M1 (see Fig. 6a), has less negative values in contrast to that of the full-atom calculations [19]. Nevertheless, the random orientation of the molecules is found at larger nitrogen-nitrogen atom distances for both models.

The atom-atom radial pair distribution function for the phenyl rings (PH1-PH2) is represented in Figure 6b. Both graphs in this figure displays the short range spatial order. The main difference between SF/M1 and SF/M2 is the amplitude of the most probable location of the first coordination shell; in the SF/M1 model this is higher than that in the SF/M2 model.

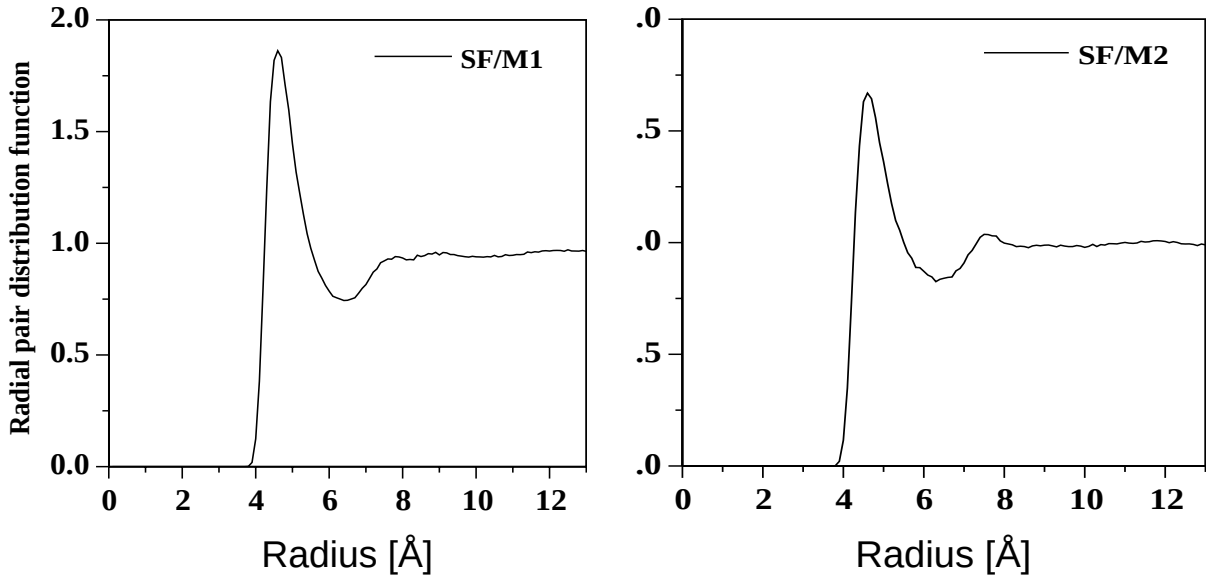

Figure 6b. Radial pair distribution function g(r) for the phenyl rings (PH1-PH2) in the isotropic state at 400 K.

The cylindrical pair distribution functions for PH1-PH2 are plotted for various values of Δz in Figure 7. The radial part at $\Delta z = 0$ looks similar to that of the radial pair distribution function (see Fig 6b). The correlation completely vanishes for higher Δz values. There are small structural differences between the models with and without electrostatic interactions.

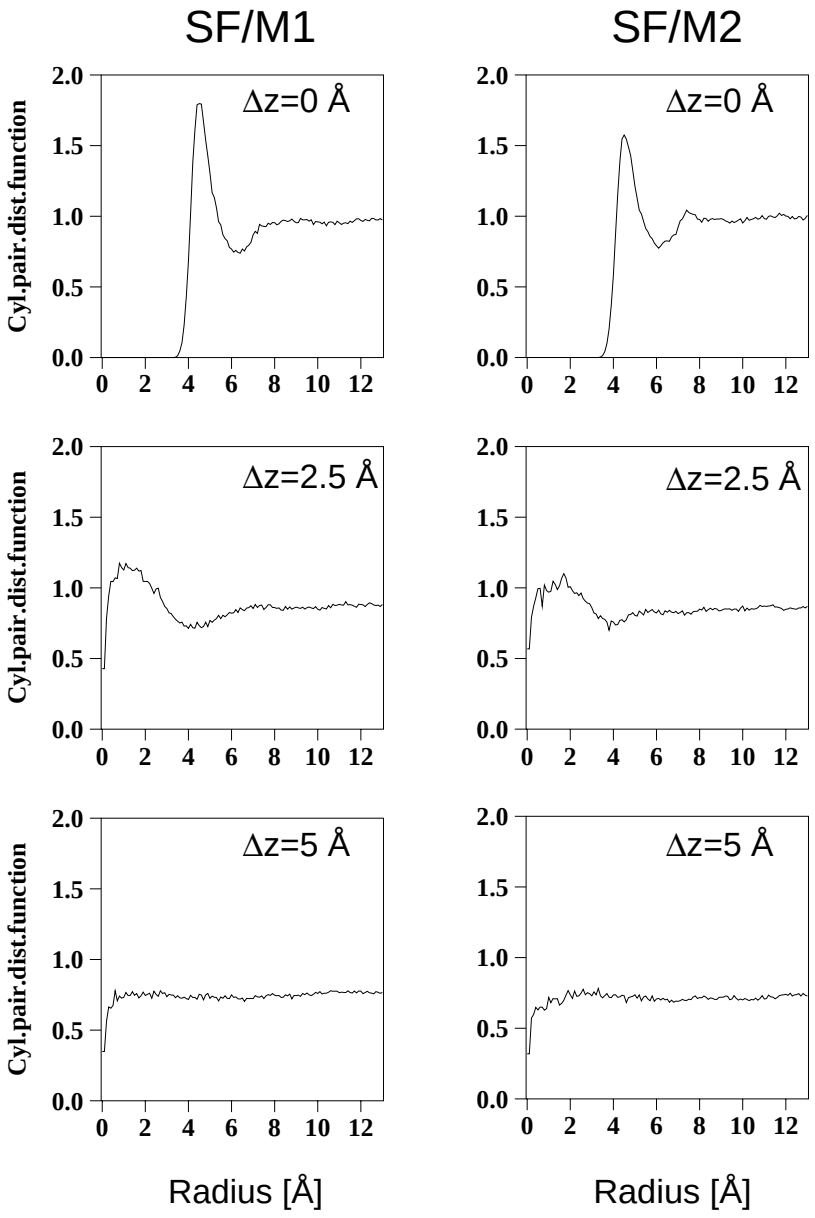

Figure 7. Cylindrical pair distribution function g(z,R) for the phenyl rings (PH1-PH2) in the isotropic state at 400 K.

4.2 Nematic State

The initial configuration of the nematic state is constructed in such a way that it contains some order, since on the time scale of the MD simulations it is difficult to observe the transitions from isotropic to ordered states [25-27]. The orientation of the molecules is chosen randomly according to the probability density function $p(\theta)$ of the long molecular axis around the direction of the preferred orientation, i.e. the director :

$$p(\grave{e}) = exp\left(-\frac{V_{ADD}}{kT}(1 - Cos^2 \grave{e}) \right), \qquad \text{Eqn (25)}$$

where θ is the angle between the director and the long molecular axis, and the constant V_{ADD} determines the initial value of the long range orientational order parameter S, which is calculated by the method of Eppenga and Frenkel [53] (see section 2.3.6).

4.2.1 Computational Details

All MD simulations have been carried out in a rectangular box with periodic boundary conditions and all trajectories are integrated by Verlet algorithm [43] with a discrete time steps of 4 fs. During the NpT simulations, the pressure, p, is set to 1 bar. Table 9 summarizes the applied NPT parameters in the nematic state.

Table 9. Parameters applied in the NpT simulations of the semi-flexible SF/M2 model and the rigid body RB/M2 model in the nematic state.

	SF/M2	RB/M2	
		Before compression	After compression
Total number of molecules	144	144	144
Temperature	330 K	330 K	300, 330,340 K
Thermostat coupling constant	0.001	0.005	0.005
Pressure coupling constant β	0.002 Pa s	0.002 Pa s	0.002 Pa s
Pressure P_o	1 bar	1 bar	1 bar
Simulation time step Δt	2 fs	2 fs	4 fs
Compression factor μ	$1*10^{-4}$	$1*10^{-4}$	$1*10^{-4}$
Cut-off Radius r_{cut}	13 Å	13 Å	13 Å

Each molecule in the semi-flexible SF/M2 model is assigned to a rectangular cell of 0.8nm x 0.8nm x 3.2nm. The center of mass is placed randomly within the cell. Considering the anisotropy of the system [26], a ratio of 4:1 between the length of the cell in the z-direction and its length along the x-and y-axis is chosen. The simulation box is made of six rectangular cells in the x-and in y-direction, and four cells in the z-direction. The conformation of the 144 molecules in the initial configuration is taken from the simulation of the liquid

state. The initial configuration has S = 0.63 and d = 0.22 g cm^{-3}. Starting from this ordered but low density configuration, the system is compressed till it reaches the experimental density of 5OCB in the nematic state at 331 K, which is 1.03 gcm^{-3} [40]. Figure 8 shows the change in order parameter with respect to the density during the compression at 330 K of the SF/M2 model. The chosen temperature is in the range of the nematic-isotropic phase transition (321-341 K) [37]. One can see that the order parameter decreases dramatically as the density increases.

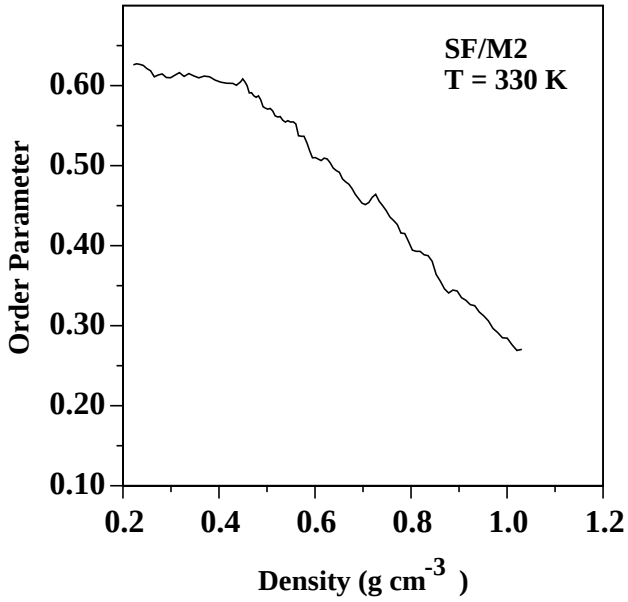

Figure 8. The change in order parameter with respect to density of the SF/M2 model during the compression at 330 K.

After compression, the NpT [48] simulation technique is applied in order to let the system relax (see Table 9). The equilibration of the system during NpT simulations can be examined by observing the changes of the order parameter S. The time evolution of the order parameter during the NpT simulation over 2.2 ns time is depicted in Figure 9. The *S* value decreases to values below 0.1 during the

first 200 ps, and remains at a very low value in the next 2 ns simulation time period. Even though the chosen temperature is in the range of the nematic state of 5OCB, the observation of such a low S value might be the consequence of the semi-flexible model, mainly because the alkyl chain is defined to be flexible.

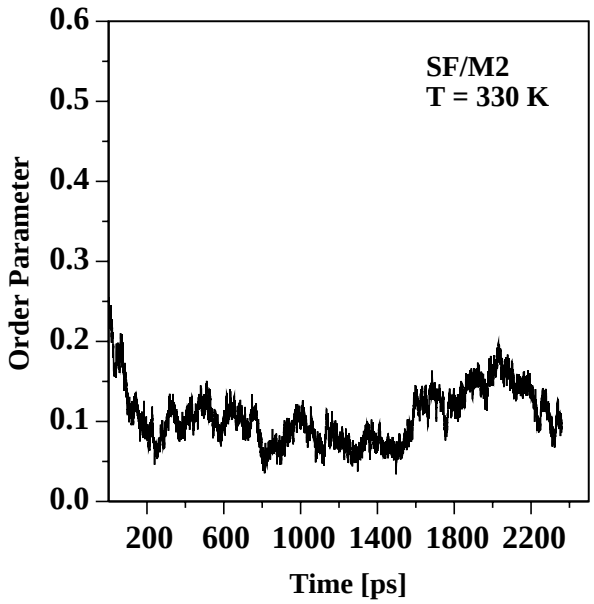

Figure 9. The time evolution of the orientational order parameter of the SF/M2 model during equilibration over a 2.2 ns NpT simulation time at 330 K.

In order to observe the influence of the molecular model on the liquid crystalline phase behavior, the semi-flexible model SF/M2 is compared to the rigid body model (RB/M2). A new simulation box is generated as mentioned above for the SF/M2 model. The only difference is the box size, which is set to be smaller in the RB/M2 model, so that a state of higher density is obtained. In this way, a highly ordered and dense configuration with S = 0.76 and d=0.99 g cm^{-3} is created. Similar to the SF/M2 case, the director is again set along the longest molecular z- axis.

The new initial structure of the RB/M2 model, which is far from equilibrium, is first equilibrated at T = 330K by NpT [48]. The change of the average order parameter with respect to time is plotted in Figure 10. It shows that the average order parameter converges to 0.79 over a 3.8 ns simulation time, while the density reaches 1.11 g cm^{-3}.

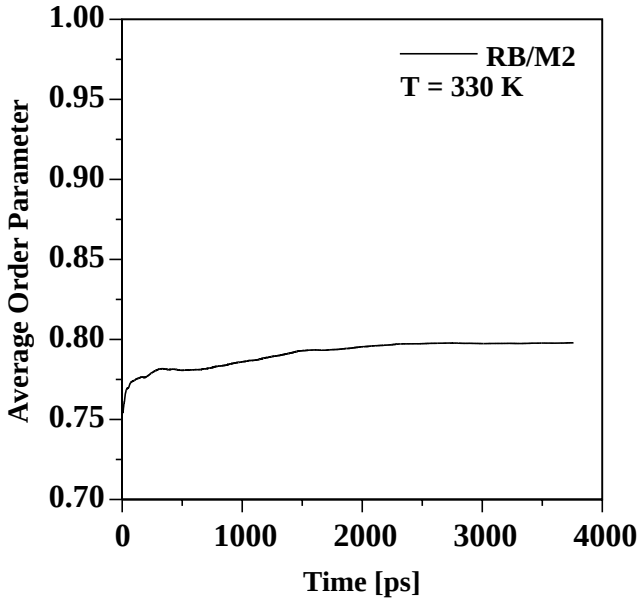

Figure 10. The time evolution of the average orientational order parameter over a 3.8 ns NpT simulation time before compression by the rigid-body RB/M2 model at 330 K.

The configuration reached after 1 ns NpT simulation with the RB/M2 model is used as an initial configuration for the SF/M2 model. During the 4.8 ns NpT simulations with SF/M2 (see Fig.11), it is seen that although the initial configuration is ordered and dense, the order parameter keeps decreasing rapidly as soon as the model is made semi-flexible. Hence, only the simulations of the

RB/M2 model are carried out in the next steps and those of the SF/M2 model are skipped from this point on.

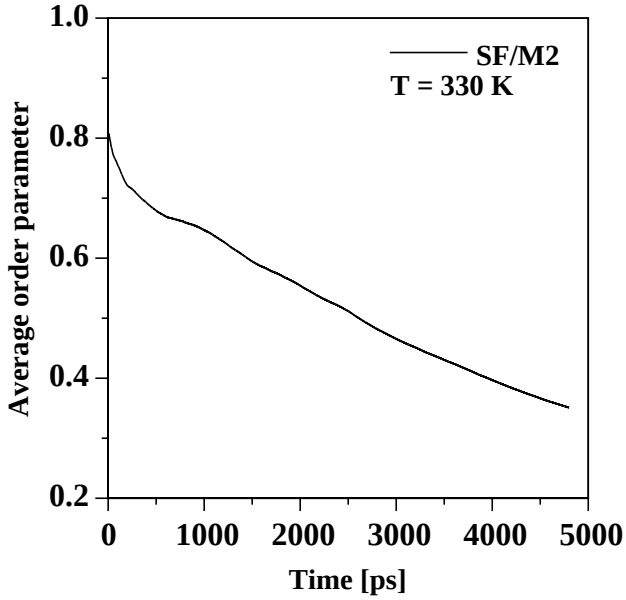

Figure 11. The time evolution of the average orientational order parameter over a 4.8 ns NpT simulation time before compression by the semi-flexible SF/M2 model at 330 K.

The equilibrated configuration of the RB/M2 model at 330 K is first compressed. After compression, the temperature is set to 300, 330 , and 340 K to examine the phase behavior of the model system as a function of the temperature and the density. Before the application of the NVT simulations [47] for the sampling, NpT simulations are carried out once more to make the system reach equilibrium after compression at 300, 330 , and 340 K respectively. In all simulations, the equilibration procedure is carried out till the average of the order parameter, box volume, potential, and kinetic energy remain constant. The main

aim of this work is to carry out longer simulations as a result of the simplifications set up in the model system so that a detailed analysis of the system can be done. The duration of the NpT simulations are nearly 17 ns at 300 K, 16 ns at 330 K, and 15 ns at 340 K, which are long enough to let the system relax and to start NVT simulations to analyze the structural and the dynamical behavior of the model system as a function of the temperature and the density. The longest simulation time carried during the MD simulations of the 5OCB by means of the full atom calculations is 1.6 ns [19].

Table 10 presents the applied NVT parameters of the rigid-body RB/M2 model during the sampling. Furthermore, a schematical representation of the computational details is exhibited in Figure 12.

Table 10 Parameters applied in the NVT simulations of RB/M2 model in the nematic state at 300, 330 and 340 K respectively.

Temperature	300 K	330 K	340 K
Thermostat coupling constant	0.0005	0.0005	0.0005
Volume	54044 $Å^3$	54967 $Å^3$	56218 $Å^3$
Simulation time	8399.2 ps	9599.2 ps	8399.2 ps

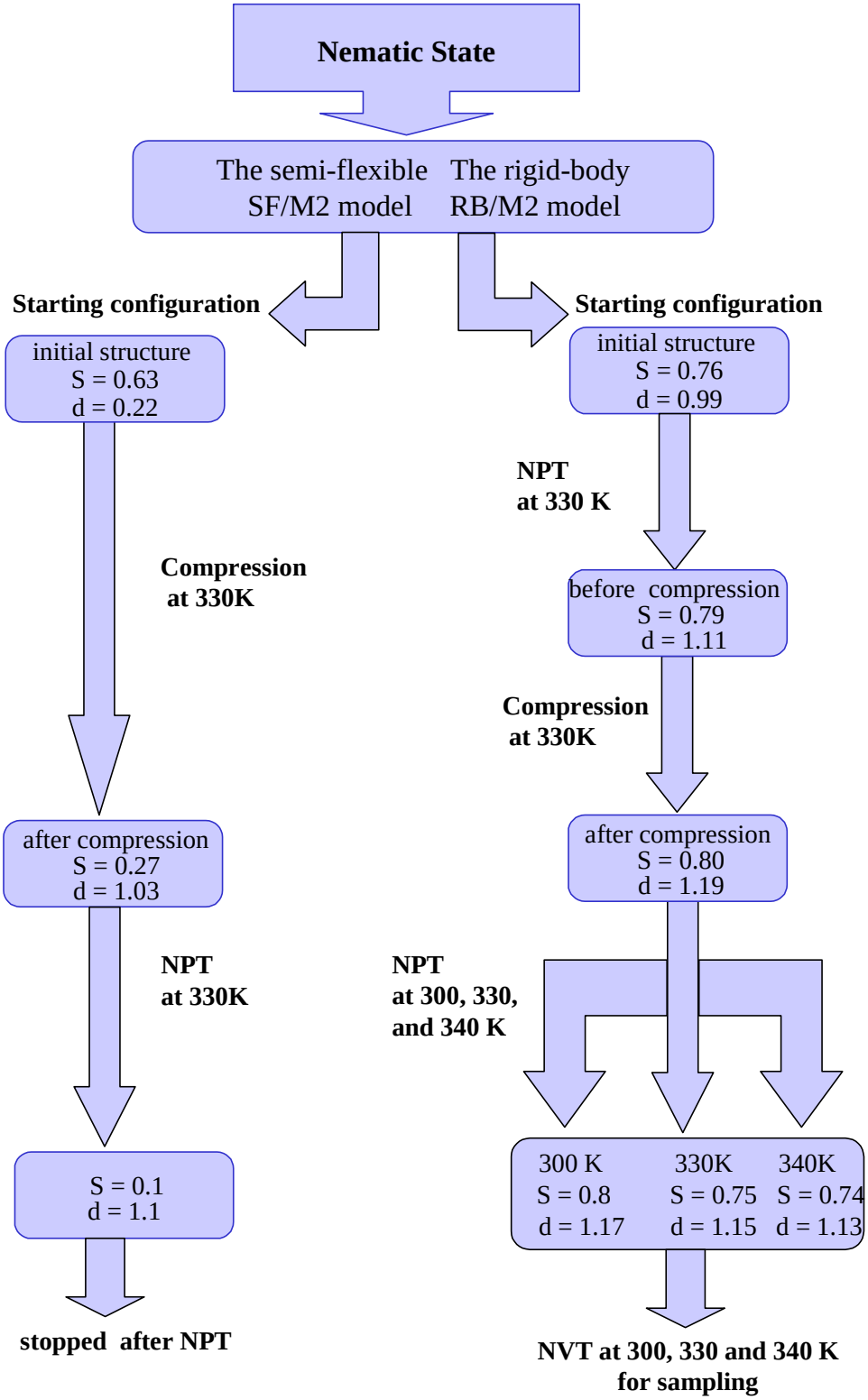

Figure 12 A schematical representation of the computational details in the nematic state. The densities (d) are in the unit of g cm^{-3} .

4.2.2 Dynamical Properties

In anisotropic systems, such as liquid crystals, anisotropy of the diffusive motion is usually observed. Especially, the self-diffusion coefficient along the director, D_{par} is greater than that perpendicular to the director, D_{per} [55].

Table 11 summarizes the calculated self-diffusion coefficients together with the order parameters and the densities obtained from the MD simulations of the RB/M2 model at 300, 330, and 340 K. Furthermore, it compares the results of the RB/M2 model to the calculated values of 5OCB by MD simulations with NVT and NPT techniques [19,20,22] in the nematic liquid crystalline state . Due to the fact that there are no experimental self-diffusion coefficient values available for 5OCB, the D_{par} and the D_{per} of 5OCB are compared to that of the 5CB molecule in the nematic state at 296.5 K [41]. The 5CB molecule differs from 5OCB in that it contains no oxygen atom.

In this work, the self-diffusion coefficients $D_{par}(D_{zz})$ and $D_{per}(D_{xx}=D_{yy})$ are calculated from the slope of the mean square displacements (MSD) of the center of mass [42]. The ratio of D_{par}/D_{per} for the RB/M2 model implies that the diffusion is faster in the longitudinal direction. There is a clear decrease in the diffusive motion of 5OCB molecules as the temperature decreases.(see Fig.13). At 300 K, the molecules can hardly diffuse. It seems that the system is in a glassy state at this temperature.

There are pronounced differences between the values obtained from the full-atom calculations (see Table 11), even though there are no big differences in the simulation techniques. The self-diffusion coefficients of the RB/M2 model are in accordance with those of the full atom calculations of 5OCB carried by Hauptmann et al. at 330 K [19]. The rate of the diffusion of the 5OCB molecule is found to be of the same order of magnitude as the 5CB molecule, which is determined by quasielastic neutron scattering (QENS) measurements [41].

Table 11 Self-diffusion coefficients parallel and perpendicular to the director, order parameters, and the densities for the nematic state of the RB/M2 model; results of the NVT simulations at 300 K, 330 K and 340 K (bold) are compared to results of the MD simulations for 5OCB at 330K [19,20] by NVT technique and 331 K [22] by NPT technique, and to the available experimentally obtained diffusion coefficients of 5CB at 296.5 K [41].

Name of the molecule	N	<T> K	<d> gcm^{-3}	S	$D_{tot}*10^{-7}$ cm^2s^{-1}	$D_{par}*10^{-7}$ cm^2s^{-1}	$D_{per}*10^{-7}$ cm^2s^{-1}	D_{par}/D_{per}
5OCB (NVT)	**144**	**300**	**1.17**	**0.81**	**0.22**	**0.45**	**0.11**	**4.09**
5OCB (NVT)	**144**	**330**	**1.15**	**0.74**	**1.95**	**3.66**	**1.09**	**3.36**
5OCB (NVT)	**144**	**340**	**1.13**	**0.70**	**3.47**	**5.29**	**2.5**	**2.07**
5OCB (NVT) [19]	144	330	1.02	0.61	3.53	6.4	2.1	3.05
5OCB (NVT) [20]	64	330		0.58	15.8	24.4	11.4	2.14
5OCB (NPT) [22]	64	331	0.98	0.53	24.5	36.0	18.8	1.91
5CB [41] Exp		296.5				5.3	4.1	1.29

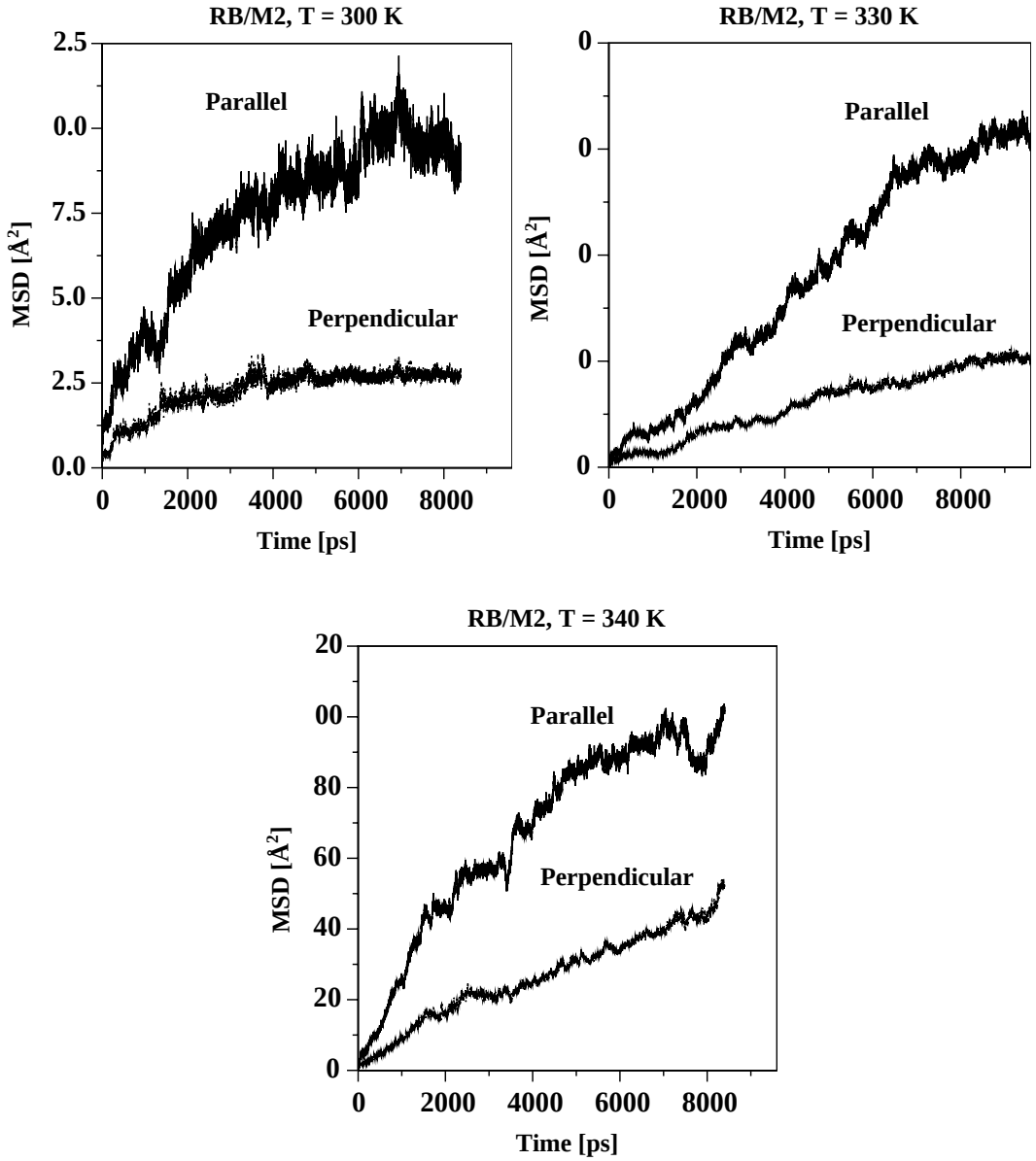

Figure 13 Mean square displacements of the molecules parallel and perpendicular to the director versus time during the NVT simulations of the RB/M2 model at 300, 330 and 340 K .

4.2.3 Structural Properties

The *nematic order* parameter is known to be temperature dependent [37,51,54]. The system for the RB/M2 model shows that the average orientational order parameter increases as the temperature decreases and the corresponding density increases (see Table 11). The experimentally determined order parameter values vary depending on the method used. The X-ray diffraction studies on the 5OCB sample, where a magnetic field was used to align the molecule, gives the *S* value of nearly 0.58 at 331 K [37]. On the other hand, the *nematic order* parameter value is found to be 0.49 at 331 K by 2D ^{13}C NMR [38] and 0.45 at 337.5 K by means of state-correlated ^{1}H two dimensional NMR spectroscopy (SC-2D) [39]. The resulting high S values of the present work are in good agreement with the Onsager theory, which explains the observance of the high order parameters in the liquid crystalline phases due to the rigidity [7].

The local structure of the nematic phase can be described by the radial pair distribution function g(r). Figure 14 depicts the radial pair distribution function between the phenyl ring of the first molecule (PH1) and that of the second molecule (PH2) at 300, 330, and 340 K respectively. The sharpness of the first peaks increases as the temperature decreases. Moreover, the short-range positional order is more pronounced in the liquid crystalline state than in the isotropic phase. Although there are pronounced peaks at large distances as well, the long-range positional order can not be discussed properly due to the finite system size, and the cut-off distance restrictions.

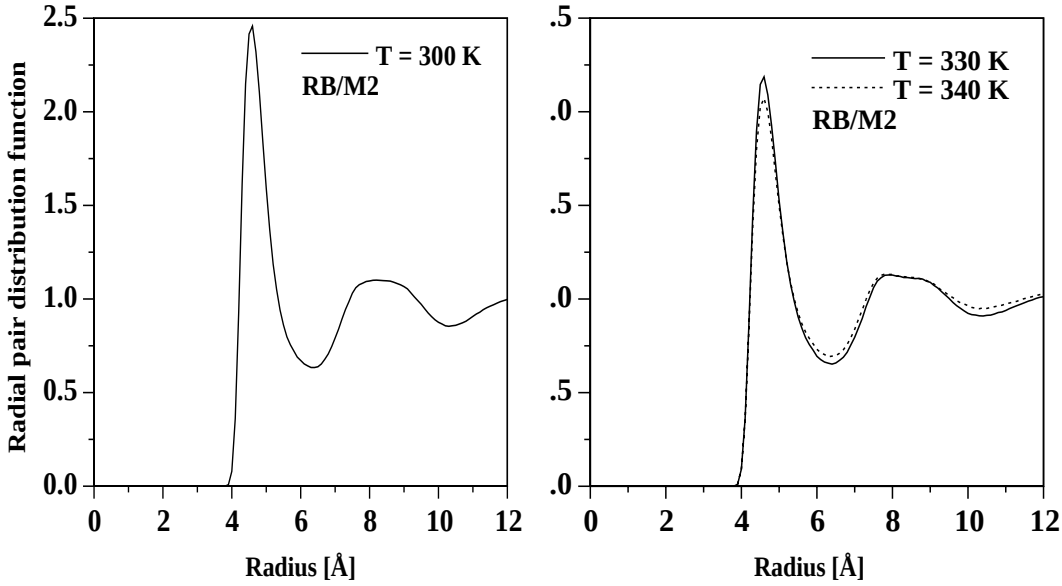

Figure 14 Radial pair distribution function g(r) for the phenyl rings (PH1-PH2) at 300, 330, and 340 K.

In order to get a more detailed picture of the local structure in the liquid crystalline state, the mutual orientation of the CN group, depending on the distances between the N-N atoms can be discussed by the angle correlation function $P_{uu}(r)$ (see Figure 15). The tendency of the antiparallel orientation of the CN groups is more pronounced than in the isotropic phase; the $P_{uu}(r)$ of the liquid crystalline state becomes more negative at short N-N distances than the corresponding function in the isotropic state.

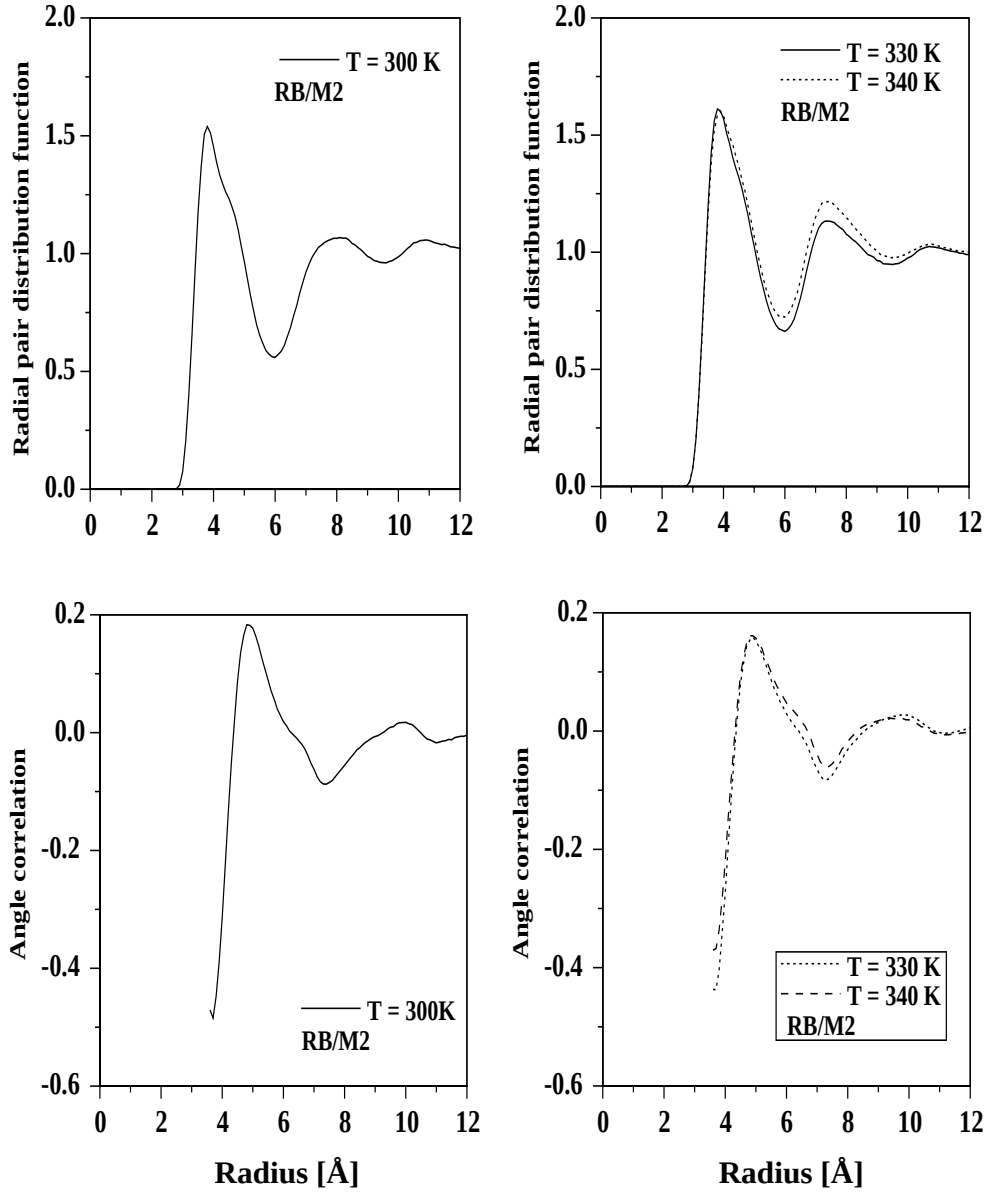

Figure 15 Radial pair distribution function g(r) of the nitrogen atoms (top) and angle correlation function $P_{uu}(r)$ for the angle between two cyano groups (bottom) depending on the N-N distances at 300, 330 and 340 K.

It is necessary to compute two resolved-component cylindrical pair distribution functions along the director and perpendicular to the director; namely g_{par} and g_{per}, in order to discriminate between possible liquid crystalline states.

Figure 16(a) represents the cylindrical pair distribution function along the director for the phenyl rings at three different temperatures. The g_{par} functions along the z-axis is in accordance with the nematic phase behavior. The small fluctuations around the value 1 are probably due to the statistical errors during the sampling. On the other hand, the g_{per} functions (Fig.16b), as well as the g(r) functions plotted in Fig. 15 show some temperature dependent pronounced peaks corresponding to the first shells of the neighboring phenyl rings. The appearance of the peaks gets sharper as the temperature decreases.

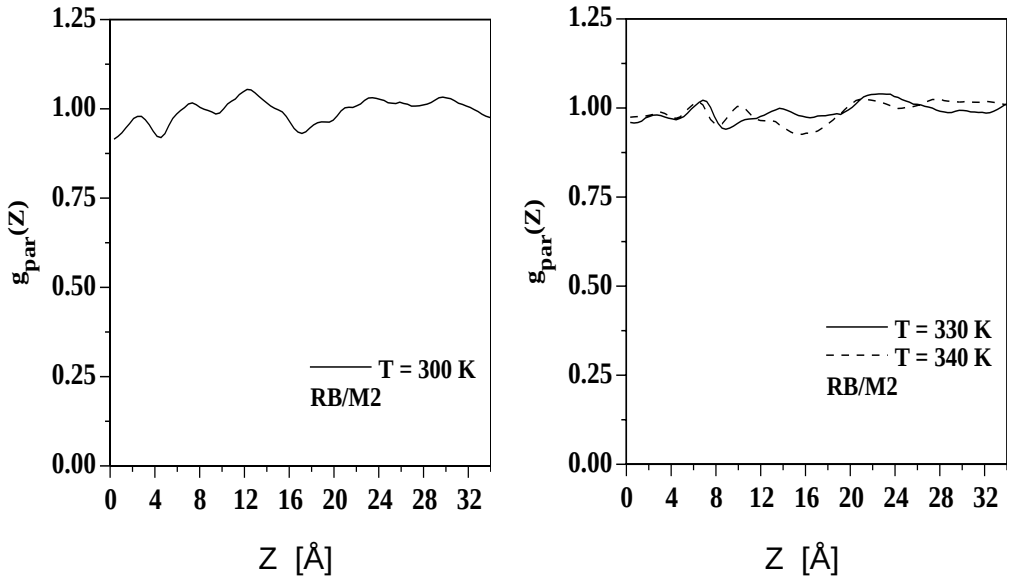

Figure 16a Cylindrical pair distribution function along the director g_{par} for the phenyl rings (PH1-PH) at 300, 330 and 340 K.

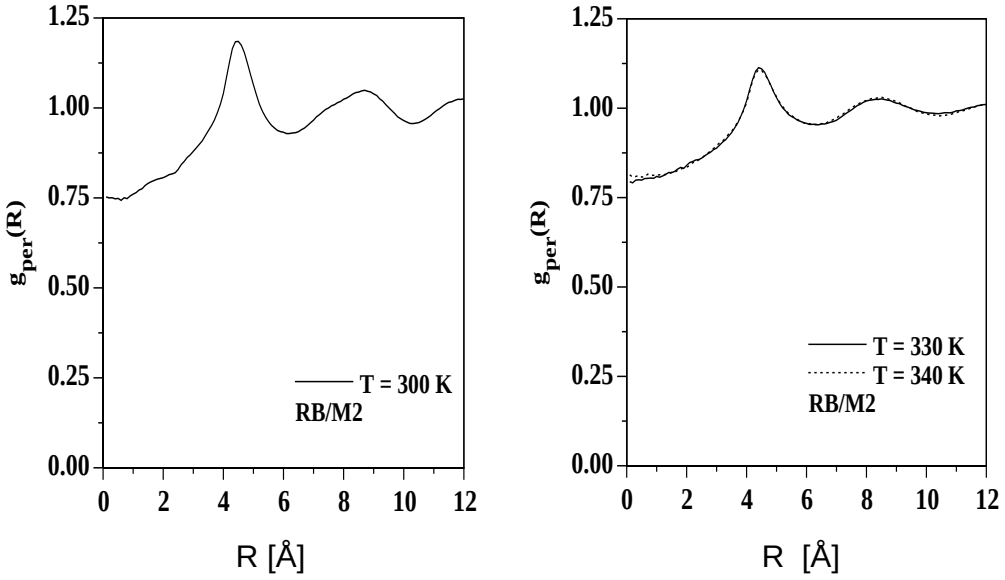

Figure 16b Cylindrical pair distribution function perpendicular to the director g_{per} for the phenyl rings (PH1-PH2) at 300, 330 and 340 K.

Not all the structural properties can be obtained from distribution functions. One can get the more detailed information about the structure from the configuration of the MD simulation runs. The snapshots of the system along the director, taken from the last configuration during the sampling with NVT simulations at 300, 330 and 340 K, are depicted in Fig. 17(a-b), 18(a-b), and Fig. 19(a-b) respectively. The angle between the director and the center of mass of each molecule are calculated to present the arrangement of the 5OCB molecules within the simulation box. There is a clear alignment of the 5OCB molecules along the director (the long molecular z axis) at all temperatures. In contrast to the system at 300 K, there are clear local cluster formations at 330 and 340 K. One can also see the appearance of the tilted boundaries between the parallel and the antiparallel arrangement of the molecules as the temperature increases.

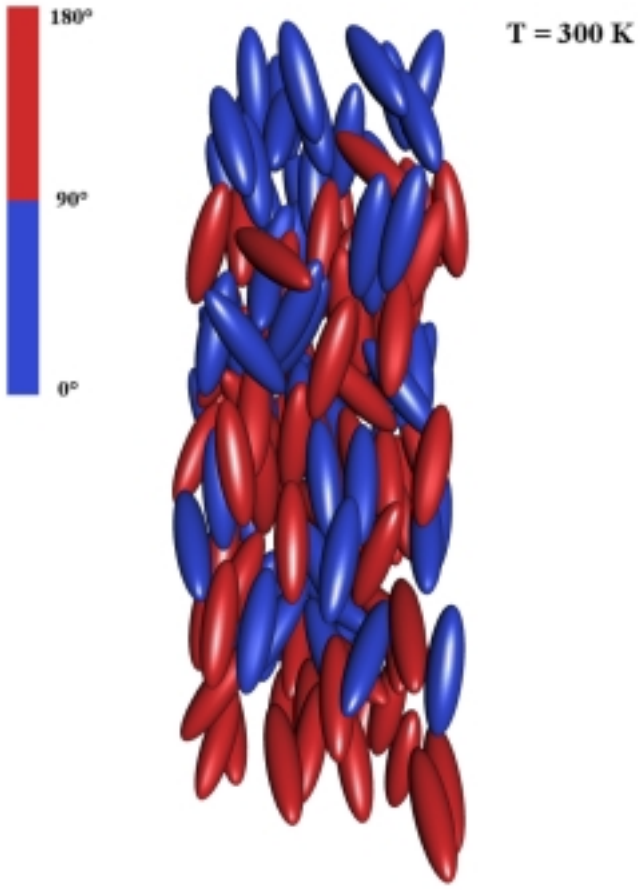

Figure 17a Snapshot of the system along the director taken from the last configuration of the sampling during the NVT simulation at 300 K, showing the parallel and the antiparallel arrangement of the 5OCB molecules.

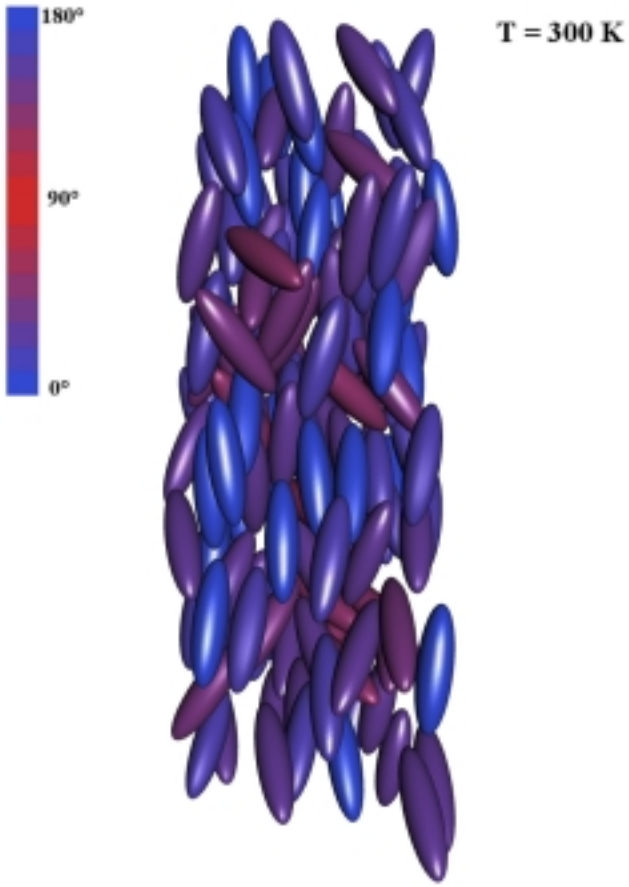

Figure 17b Snapshot of the system along the director taken from the last configuration of the sampling during the NVT simulation at 300 K.

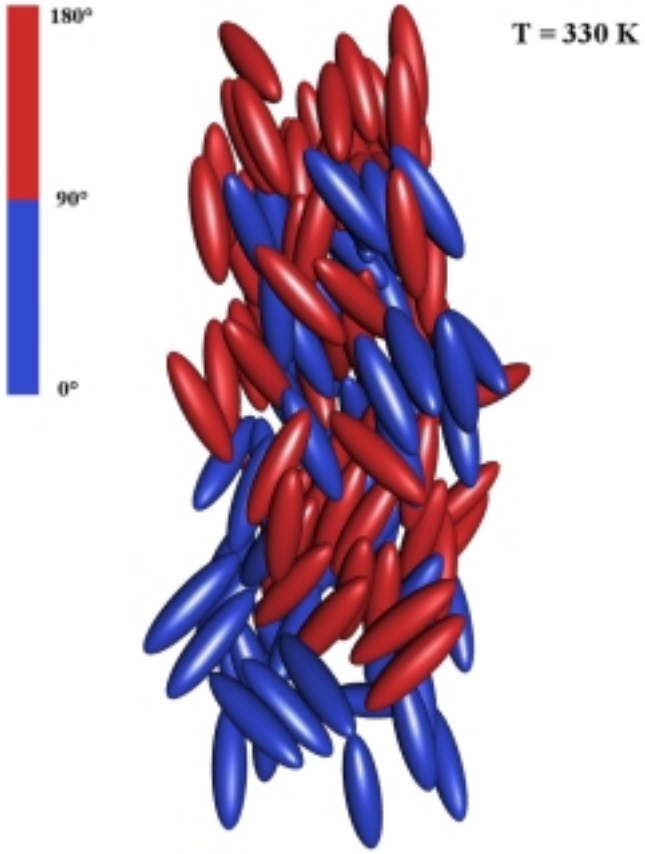

Figure 18a Snapshot of the system along the director taken from the last configuration of the sampling during the NVT simulation at 330 K, showing the parallel and the antiparallel arrangement of the 5OCB molecules.

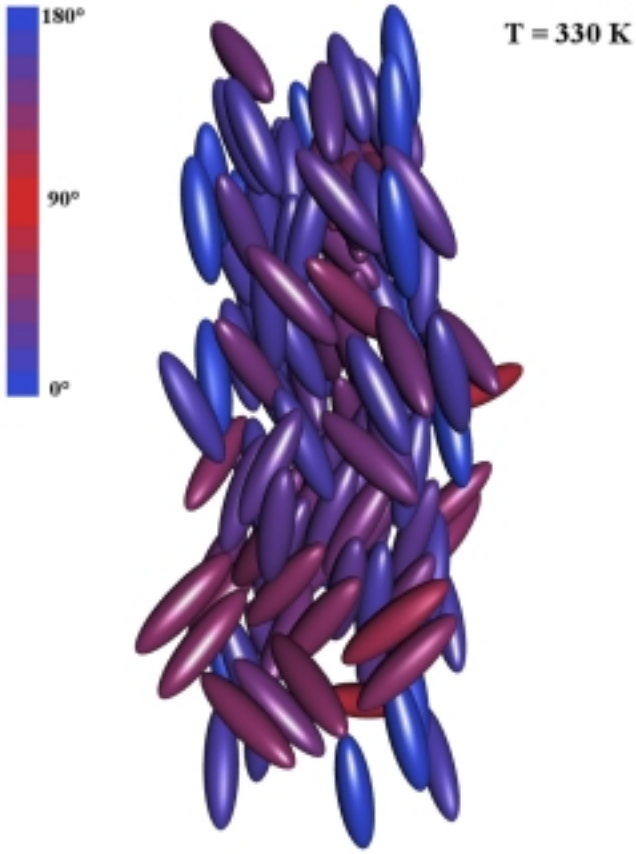

Figure 18b Snapshot of the system along the director taken from the last configuration of the sampling during the NVT simulation at 330 K.

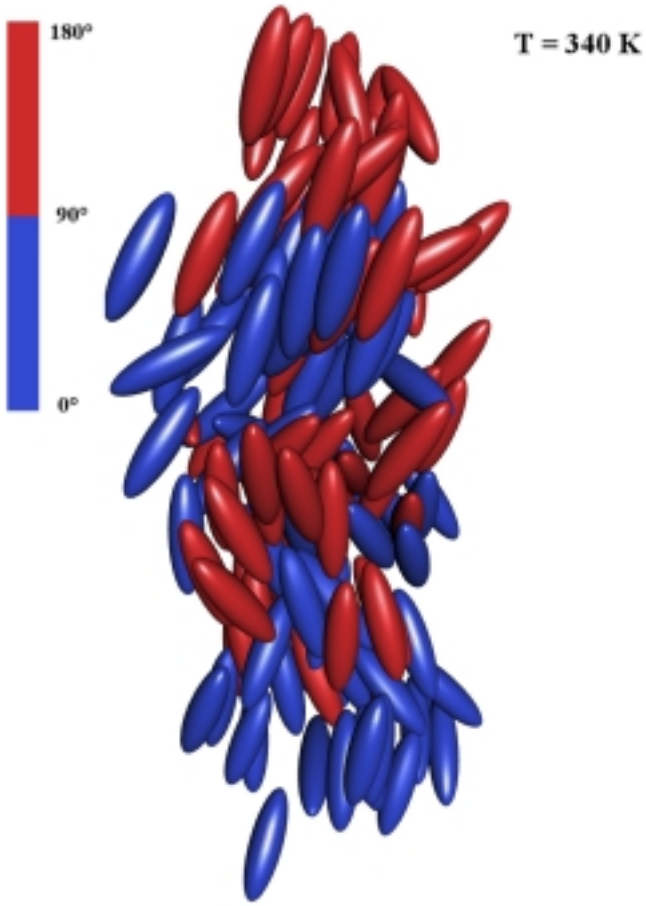

Figure 19a Snapshot of the system along the director taken from the last configuration of the sampling during the NVT simulation at 340 K, showing the parallel and the antiparallel arrangement of the 5OCB molecules.

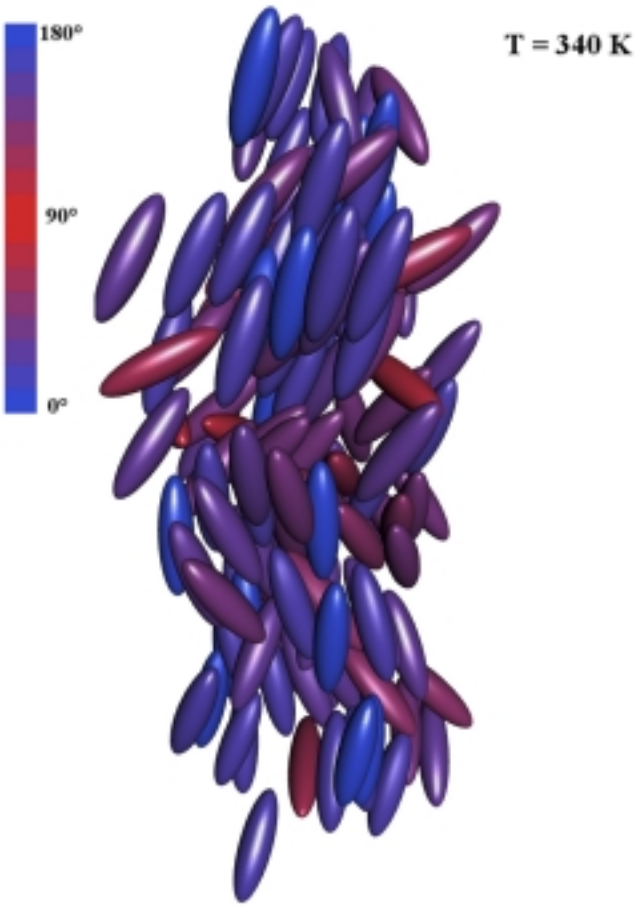

Figure 19b Snapshot of the system along the director taken from the last configuration of the sampling during the NVT simulation at 340 K.

CHAPTER V

CONCLUSION

There are several levels of sophistication in the MD simulations of liquid crystals, such as simple rods, flexible chains connected to rigid cores, and full atom-atom potentials. The last approach, realistic full atom-atom potential, is the most sophisticated one, and has been employed in the MD simulations of the various liquid crystals. However, the drawback of the realistic models with the use of full atom-atom potentials is that they are extremely expensive in terms of computational time. Thus, there is a need for less complex models, which will reduce the computational time considerably but still allow to analyze the structural and the dynamical properties of the examined phase.

In this work, the influence of the force-field parameters on the isotropic and the liquid crystalline phase behavior of the simplified molecular model system for 5OCB has been investigated by means of MD simulations.

The simplified models are named as the semi-flexible SF/M1 model, the semi-flexible SF/M2 model, and the rigid-body RB/M2 model. In the SF/M1 model, the electrostatic interactions are excluded in contrast to the SF/M2 and the RB/M2 models. The part of the 5OCB molecule from N to O atom is kept rigid in both the SF/M1 and the SF/M2 model, while the alkyl chains are kept flexible. On the other hand, the RB/M2 model is defined to be completely rigid. The RB/M2

model is the modification of the SF/M2 model in a way that the interaction potential consists of only the non-bonded interactions. The charges in the SF/M2 and, thus in the RB/M2 model, are set only on the part of the 5OCB molecule from N to O atom. In all three models, the bond lengths are constrained and each phenyl ring is treated as a *sphere* [36], modeled as *a united atom*, which reduces the total number of "*atoms*" in the system with a consequent reduction in computational time.

The use of the SF/M1 and the SF/M2 model in the isotropic phase of the 5OCB molecule shows that the structural properties are not much effected due to the inclusion or the exclusion of the electrostatic interactions which is indicated by the similar distribution functions and the order parameters of the two models. Concerning the dynamical properties of the system, on the other hand, it looks like that the system is rigid, a kind of a "*glass*" like state. Nevertheless, the low values of the order parameters, the preference of the random orientation of the molecules at large distances, and a nearly uniform distributions of the molecular orientation can be considered for the presence of the isotropic phase of both models.

In the nematic liquid crystalline state, the influence of the semi-flexibility and the rigidity are examined by means of the SF/M2 and the RB/M2 models respectively. The SF/M1 model, where the electrostatic interactions are excluded, is not considered in the nematic phase since first of all no significant differences have been observed between the SF/M1 and the SF/M2 models in the isotropic state and second of all it is more realistic to include the electrostatic interactions.

The initial configuration of the nematic state is prepared to have some order since it is difficult to observe the transitions from isotropic state to ordered states on the time scale of the MD simulations. It is found that during the equilibration in the nematic state, the introduction of the semi-flexibility causes a very rapid decrease in the orientational order parameter to a value of 0.1 although the starting configuration has some initial order. The flexible alkyl chain is probably the reason for such an unexpectedly low value for the nematic phase. Therefore, the simulations of the SF/M2 model are stopped after the equilibration. In the further steps only the effect of the RB/M2 model has been examined on the nematic phase behavior of 5OCB as a function of temperature and density. Due to the simplifications set up in the model system , it was possible to carry out long simulations varying between 3.8 ns and 17 ns depending on the simulation procedure applied. In the literature, the longest MD simulation time for the same system is 1.6 ns with the use of full-atom calculations [19].

As a result of the NVT simulations for the sampling, dynamical properties show that the diffusion is faster along the longitudinal direction at all temperatures in the nematic state. The rate of diffusion of 5OCB molecules is increasing with the increasing temperature. The values are in the same order of magnitude with these of the full atom calculations of the same system [19].

There is a tendency of increasing the orientational order parameter as the temperature decreases and the corresponding density increases. The obtained high order parameters can be interpreted by the Onsager theory [7], which explains the observance of the high order parameters due to rigidity in the liquid crystalline

phases. The pronounced antiparallel orientation of the molecules, as well as the observation of the stronger short range order in the nematic state than in the isotropic state are in a good agreement with the results of the full atom calculations carried by Hauptmann et al. [19]. In order to discriminate between possible liquid crystalline states, the cylindrical pair distribution functions along the director (the longest molecular z axis), g_{par}, and perpendicular to the director, g_{per}, are also calculated. The structure of the g_{par}, is in accordance with the nematic phase behavior and that of the g_{per} shows some temperature dependent pronounced peaks corresponding to the first coordination shells. Although there are also peaks observed at long distances in the g_{per} functions as well as in the radial pair distribution functions, one can not conclude for the presence of the long range order due to the small system size and the truncation of the intermolecular potential at a certain spherical cutoff distance, which restricts the total number of interactions.

One can gain the most detailed structural information from the configuration of the system during the simulation runs. The snapshots taken from the last configuration of the NVT simulations reveal the alignment of the molecules along the director at all temperatures. Going from the lowest temperature system to the next highest one, tilted boundaries occur between the parallel and the antiparallel arrangement of the molecules. It looks like that there is a beginning of a phase transition from the solid phase to the nematic liquid crystalline phase as the temperature changes from 300 K to 330 K. There are clear local cluster formations as the temperature increases, which has not been

examined until now neither by experimental nor theoretical studies in the liquid crystalline systems, but it has been the topic of recent discussions. It is advisable to divert some interest for the further studies of the liquid crystalline systems in this direction as well.

CHAPTER VI

ZUSAMMENFASSUNG

1 Einleitung

Die flüssigkristalline Phase bildet hinsichtlich ihrer Eigenschaften einen besonderen Aggregatzustand zwischen der kristallinen, festen und der amorphen, flüssigen Phase [1-3]. Einige Eigenschaften von Flüssigkristallen sind stark anisotrop ausgeprägt. Auf der anderen Seite zeigen diese Substanzen auch einen starken Grad an Fluidität, der in manchen Fällen mit dem normaler Flüssigkeiten vergleichbar ist. Flüssigkristalle bzw. mesomorphe Eigenschaften wurden zuerst von Reinitzer im Jahr 1888 [4] und Lehmann um 1890 [5] beobachtet. Eine essentielle Voraussetzung für die Ausbildung mesomorpher Eigenschaften ist die starke strukturelle Anisotropie der Moleküle. Die Systeme können eine oder mehrere mesomorphe Phasen ausbilden, bevor die isotrope, flüssige Phase erreicht wird. Die Umwandlungen zwischen diesen mesomorphen Zuständen können durch reine thermische Prozesse (*thermotrope Mesomorphie*) oder durch den Einfluß des Lösungsmittels (*lyotrope Mesomorphie*) hervorgerufen werden.

Thermotrope Flüssigkristalle werden nach Friedel [6] grob in drei Klassen unterteilt: nematisch, cholesterisch und smektisch.

Nematische Flüssigkristalle zeigen eine starke Fernordnung der Molekülorientierung, ohne eine Anordnung auf einem dreidimensionalen

Translationsgitter zu besitzen. Sie unterscheiden sich von der isotropen, flüssigen Phase durch eine nahezu parallele Ausrichtung der Längsachse der Moleküle. Nematische Phasen können somit von Molekülen mit einer mehr oder weniger ausgeprägten langgestreckten, stäbchenartigen Form gebildet werden. Die cholesterische Phase ist ebenfalls ein nematischer Typ von Flüssigkristall. Die Moleküle weisen aber zusätzlich optische Aktivität auf. In smektischen Flüssigkristallen wird das System aus zweidimensionalen fluiden Schichten, die in einem definierten Abstand übereinander angeordnet sind, aufgebaut.

Flüssigkristalline Systeme fanden in den letzten 20 Jahren starkes Interesse. Dies ist nicht nur auf die große Anzahl technischer Einsatzgebiete, wie z.B. Flüssigkristallanzeigen (LCD) für Uhren, Taschenrechner, Bildschirme und molekulare Schalter usw. zurückzuführen, sondern auch auf die große Rolle, die sie bei der Aufklärung des kooperativen Verhaltens von Molekülen und dessen Ursachen spielen.

Das Verhalten der flüssigkristallinen Phase wird durch die Moleküleigenschaften, wie z.B. Gestalt, Flexibilität, Ladungsverteilung und Polarisierbarkeit, bestimmt. Theoretische Untersuchungen flüssigkristalliner Phasen haben eine lange, auf Onsager [7] zurückgehende, Geschichte. Frühe Arbeiten von Maier und Saupe [8-11] wurden häufig benutzt, um die Eigenschaften von Flüssigkristallen zu charakterisieren. Diese Theorie basiert auf der Beschreibung des flüssigkristallinen Moleküls als starres Stäbchen, das über ein effektives Potential mit den umgebenden Molekülen wechselwirkt. Die von den flexiblen Alkylketten

hervorgerufenen Anteile wurden zuerst von Marcelja berücksichtigt [12]. Obwohl diese Theorien viele Eigenschaften der Flüssigkristalle erklären können, sind sie nicht in der Lage, das beobachtete Verhalten der Phase mit den detaillierten Strukturcharakteristika und den Moleküleigenschaften zu korrelieren.

Verbindungen wie 4-Cyano-4'-*n*-alkyloxybiphenyl (nOCB) oder 4-Cyano-4'-*n*-alkylbiphenyl (nCB), wobei *n* für die Anzahl von Kohlenstoffatomen in der Alkyloxy- bzw. Alkyl-Kette steht, sind als stäbchenartige Moleküle bekannt. Die langgestreckte, anisotrope Geometrie ermöglicht die bevorzugte Ausrichtung entlang einer Raumrichtung [13]. Diese Verbindungen sind von breitem wissenschaftlichen Interesse sowohl als reine Phase als auch in Lösung. Außerdem werden sie in kommerziellen Mischungen für LCDs verwendet [14]. Kristall- und Molekülstrukturen einiger dieser Verbindungen (nOCB mit n = 2,3,4 und nCB mit n = 2,3,5) wurden von Haase und Mitarbeitern untersucht [15-18]. Neben diesen experimentellen Arbeiten beschäftigten sich viele computergestützte Untersuchungen mit Flüssigkristallen. Eine Reihe dieser Arbeiten wurden unter vollständiger Berücksichtigung der inneren Freiheitsgrade der flüssigkristallinen Materialien mit Molekulardynamik- (MD) und Monte-Carlo-(MC) Simulationen durchgeführt [19-29]. Realistische Modelle von Substanzen wie 5OCB [19,20,22] und 5CB [23] sind aber sehr rechenintensiv und erreichen dadurch die Grenzen der Leistungsfähigkeit heutiger Computer. Darum wurden weniger komplexe Modelle in MD- und MC-Simulationen verwendet, die die wichtigsten der oben erwähnten molekularen Eigenschaften und deren Auswirkungen auf das flüssigkristalline Verhalten berücksichtigen sollen [30-36].

Das Ziel der vorliegenden Arbeit bestand in der Untersuchung des Einflusses der Kraftfeld-Parameter auf das Verhalten der isotropen und flüssigkristallinen Phase des Modellsystems 5OCB mit Hilfe von MD-Simulationen. Die Phasenabfolge des 5OCB verläuft von der kristallinen über eine nematische zur isotropen Phase [37]. Die Untersuchungen des Phasenverhaltens des 5OCBs mit MD-Simulationen unter Berücksichtigung sämtlicher molekularer Freiheitsgrade ist durch den hohen Rechenaufwand auf eine kurze Simulationszeit begrenzt [19,20,22]. Deswegen wurde in der hier vorgestellten Arbeit eine Reihe von Vereinfachungen am Modellsystem zur Beschreibung des Phasenverhaltens des 5OCB eingeführt. Dazu zählen die Beschreibung des Phenylrings im Rahmen eines *united atom*-Ansatzes durch eine Kugel [36], die Vernachlässigung der elektrostatischen Wechselwirkungen und die Behandlung des 5OCB-Moleküls als Starrkörper oder teilflexibles Modell. Diese Vereinfachungen ermöglichen eine längere Simulationszeit, wodurch die dynamischen und die strukturellen Eigenschaften, wie z.B. der Diffusionskoeffizient, die Ordnungsparameter sowie die Orts- und Zeitkorrelationsfunktionen sowohl der isotropen als auch der flüssigkristallinen Phase des 5OCBs als Funktion der Temperatur und der Dichte untersucht werden konnten. Zusätzlich konnten diese Simulationen im Falle von Ordnungsparameter, Dichte und Selbstdiffusionskoeffizienten mit den Ergebnissen aus Simulationen unter Berücksichtigung sämtlicher Freiheitsgrade sowie mit experimentellen Werten verglichen werden.

2 Ergebnisse

Es existieren verschiedene Stufen von Modellansätzen zur Beschreibung von Flüssigkristallen in MD-Simulationen: einfache Fäden, flexible Seitenketten an einem starren Grundgerüst bzw. Atom-Atom-Potentiale unter Berücksichtigung der gesamten Flexibilität sind Beispiele hierfür.

Der letztgenannte Ansatz ist der realitätsnahste und wurde deswegen in MD-Simulationen verschiedenster Flüssigkristalle häufig verwendet. Der Nachteil dieses Modells ist der hohe Aufwand an Rechenleistung. Daher besteht ein Bedarf an vereinfachten Modellen, die eine Reduzierung der benötigten Rechenzeit erlauben, aber trotzdem die strukturellen und dynamischen Eigenschaften der untersuchten Phase mit ausreichender Genauigkeit beschreiben.

In der vorliegenden Arbeit wurde im Rahmen von MD-Simulationen der Einfluß der Kraftfeld-Parameter auf das Verhalten der isotropen und flüssigkristallinen Phase für ein vereinfachtes, molekulares Modell des 5OCB-Systems untersucht.

Die vereinfachten Modelle werden in dieser Arbeit als semi-flexibles SF/M1-, semi-flexibles SF/M2- und starres RB/M2-Modell bezeichnet. Im SF/M1-Modell werden die elektrostatischen Wechselwirkungen im Gegensatz zu den SF/M2- und RB/M2-Modellen vernachlässigt. Die Alkylkette des 5OCB-Moleküls ist sowohl im SF/M1-, wie auch im SF/M2-Modell flexibel, während der Rest des Moleküls jeweils starr bleibt. Im RB/M2-Modell wird das Molekül als Starrkörper behandelt. Das RB/M2-Modell ist insoweit eine Modifikation des SF/M2-Modells, als das Wechselwirkungspotential für die nichtbindenden

Wechselwirkungen in beiden Modellen identisch sind. Weitherhin werden im SF/M2- und somit auch im RB/M2-Modell die Partialladungen des Alkylrests vernachlässigt. In allen drei Modellen werden die Bindungslängen konstant gehalten und die Phenylringe im Rahmen eines *united atom*-Ansatzes durch eine Lennard-Jones-Kugel ersetzt. Dadurch wird die Gesamtzahl von Atomen sowie die Zahl der Freiheitsgrade im System verringert und eine Reduktion des Rechenaufwandes erzielt.

Die Verwendung des SF/M1- und SF/M2-Modells für die isotrope Phase zeigten, daß die strukturellen Eigenschaften der Flüssigkeit nur wenig durch die explizite Berücksichtigung bzw. Vernachlässigung der elektrostatischen Wechselwirkungen beeinflußt wird. Dies zeigt sich in den ähnlichen Paarverteilungsfunktionen und Ordnungsparametern für die beiden Modelle. Die Untersuchungen von dynamischen Eigenschaften ergaben, daß sich das System in einem starren, eher als *glasartig* zu bezeichnenden Zustand befindet. Trotzdem können die niedrigen Werte für die Ordnungsparameter und die nahezu gleichmäßige Verteilung der Molekülorientierungen in beiden Modellen als Argumente für die Existenz einer isotropen Phase herangezogen werden.

Im nematischen, flüssigkristallinen Zustand wurde der Einfluß der Semiflexibilität bzw. Rigidität des Moleküls mit Hilfe des SF/M2- bzw. RB/M2-Modells untersucht. Das SF/M1-Modell, in dem die elektrostatischen Wechselwirkungen vernachlässigt wurden, fand in den Simulationen der nematischen Phase keine Anwendung, da erstens keine signifikanten Unterschiede zwischen dem SF/M1- und SF/M2-Modell in der isotropen Phase erkannt werden konnten und zweitens

durch die Berücksichtigung der elektrostatischen Wechselwirkungen eine realistischere Beschreibung des Systems in der flüssigkristallinen Phase erfolgen soll.

Da der Phasenübergang flüssig-flüssigkristallin innerhalb des aus MD-Simulationen zugänglichen Zeitfensters nicht beobachtet werden kann, wurde die Ausgangskonfiguration der nematischen Phase bereits mit einer gewissen Vorordnung aufgebaut. Es zeigte sich während der Gleichgewichtseinstellung in der nematischen Phase, daß die Einführung der Semiflexibilität trotz der anfänglichen Ordnung eine starke Abnahme des Ordnungsparameters auf einen Wert von 0.1 zur Folge hat. Die flexiblen Alkylketten sind vermutlich die Ursache für diesen zu niedrigen Wert in der nematischen Phase. Daher wurden die Simulationen mit dem SF/M2-Modell nach Erreichen des Gleichgewichtzustandes beendet. In den nächsten Schritten wurde der Einfluß des RB/M2-Modells auf das Verhalten der nematischen Phase von 5OCB als Funktion der Temperatur und der Dichte untersucht. Durch die Vereinfachungen des Modellsystems war es möglich, die Simulationen über einen Zeitraum von 3.8 ns bis 17 ns, abhängig von der Simulationsart, durchzuführen. Die längste, bislang veröffentlichte Simulationsdauer für dieses System mit voller Flexibilität betrug hingegen nur 1.6 ns [19].

Die Auswertung der Simulationen bei konstanter Dichte und Temperatur (NVT) zeigten, daß die Diffusion in der nematischen Phase für alle Temperaturen entlang der Moleküllängsachse am schnellsten verläuft. Der Diffusionskoeffizient des

5OCBs steigt mit höherer Temperatur an. Die Werte liegen in derselben Größenordnung wie die in den Simulationen mit voller Flexibilität [19].

Es zeigte sich außerdem eine Zunahme des Ordnungsparameters bei abnehmender Temperatur und zunehmender Dichte. Die höheren Werte des Ordnungsparameters können mit der Onsager-Theorie [7], die das Auftreten hoher Ordnungsparameter mit der Rigidität in der Flüssigkristallphase korreliert, erklärt werden. Die ausgeprägte antiparallele Ausrichtung der Moleküle sowie die verglichen mit der isotropen Phase stärkere Nahordnung in der nematischen Phase ergeben eine gute Übereinstimmung mit den Ergebnissen von Hauptmann et al. [19] am vollflexiblen Modell. Um zwischen möglichen flüssigkristallinen Zuständen zu unterscheiden, wurden die Paarverteilungsfunktionen parallel (g_{par}) und senkrecht (g_{per}) zum Direktor (längste Molekülachse) berechnet. Die Funktion g_{par} zeigt eine Fluktuation um den Wert von 1 und ist damit im Einklang mit dem Verhalten einer nematischen Phase. Die Struktur von g_{per} zeigt ausgeprägte, temperaturabhängige Spitzen, die der ersten Koordinationssphäre entsprechen. In der g_{per}-Funktion sowie bei den radialen Paarverteilungsfunktionen treten auch bei weiteren Entfernungen Maxima auf. Wegen der Begrenztheit des Systems und der Verwendung eines intermolekularen Potentials mit *cutoff* kann aus der Verteilungsfunktion jedoch nicht auf eine Fernordnung der Moleküle geschlossen werden.

Die detailiertesten, strukturellen Informationen können aus der Konfiguration des Systems währen der Simulation erhalten werden. Die Momentaufnahme der

letzten Konfiguration der NVT-Simulationen bestätigen bei allen Temperaturen die Ausrichtung der Moleküle entlang des Direktors. Beim Übergang von der niedrigsten zur nächsthöheren Temperatur weisen die Grenzen zwischen den parallelen und antiparallelen Anordnungen der Moleküle einen Neigungswinkel auf. Bei einer Änderung der Temperatur von 300 K auf 330 K lassen sich in Rahmen der Simulationen Anzeichen für den Phasenübergang kristallin-nematisch beobachten. Allgemein kommt es bei Temperaturerhöhung zur Ausbildung von Clustern, was jedoch bislang weder in experimentellen noch in theoretischen Untersuchungen flüssigkristalliner Systeme beobachtet wurde. Dieses interessante Phänomen ist gegenwärtig in der Diskussion.

CHAPTER VII

REFERENCES

[1] Chandrasekhar, S., *Liquid Crystals*, Cambridge University Press (1977).

[2] Priestly, E.B., Wojtowicz, P.J., and Sheng, P., *Introduction to Liquid Crystals*, Plenum Press, New York (1974).

[3] Baumgaertel, H., Franck, E.U., and Gruenbein, W., *Liquid Crystals*, Steinkopf Darmstadt-Springer New York (1994).

[4] Reinitzer, F., *Montash Chem.*, **9**, 421 (1888).

[5] Lehmann, O., Z. *Krist.*, **18**, 464 (1890).

[6] Friedel, G., *Ann. Physique*, **18**, 273 (1922).

[7] Onsager, L., *Ann.N.Y.Acad.Sci.*, **51**, 627 (1949).

[8] Maier,W., and Saupe,A., *Naturforsch. Teil A*, **13**, 564 (1958).

[9] Maier,W., and Saupe,A., *Naturforsch. Teil A*, **14**, 1909 (1959).

[10] Maier,W., and Saupe,A., *Naturforsch. Teil A*, **15**, 282 (1960).

[11] Saupe,A., *Angew. Chem. Int. Ed.*, **7**, 97 (1968).

[12] Marcelja, S., *J.Chem.Phys.*, **60**, 3599 (1974).

[13] Crain, J., Clark, S.J.: Calculation of Structure and Dynamical Properties of Liquid Crystal Molecules. In : *Structure and Bonding, Liquid Crystals I* (Ed. Mingos, D.M.P.), pp. 2-38, Springer–Verlag, Berlin, Heidelberg, (1999).

[14] Haase, W., Private Communications.

[15] Walz, L., Paulus, H., and Haase, W., *Z. Kristallogr*., **180**, 97 (1987).

[16] Haase, W., Loub, J., and Paulus, H., *Z. Kristallogr*., **202**, 7 (1992).

[17] Hanemann, T., Haase, W., Svoboda, I., and Fuess, H., *Liq. Cryst.*, **19** (5), 699 (1995).

[18] Haase, W., Athanassopoulou, M. A.: Crystal Structures of LC Mesogens. In : *Structure and Bonding, Liquid Crystals I* (Ed. Mingos, D.M.P.), pp. 140-193, Springer– Verlag, Berlin, Heidelberg, (1999).

[19] Hauptmann, S., Mosell, T., Reiling, S., and Brickmann, J., *Chem. Phys.*, **208**, 57 (1996).

[20] Ono, I., and Kondo, S., *Mol. Cryst. Liq. Cryst. Lett.*, **8** (4), 69 (1991).

[21] Ono, I., and Kondo, S., *Bull. Chem. Soc. Jpn.*, **65**, 1057 (1992).

[22] Ono, I., and Kondo, S., *Bull. Chem. Soc. Jpn.*, **66**, 633 (1993).

[23] Picken, S.J., Van Gunsteren, W.F., Van Duijnen, P.Th., and De Jeu, W.H., *Liq. Cryst.*, **6** (3**)**, 357 (1989).

[24] Wilson, M.R., and Allen, M.P., *Mol. Cryst. Liq. Cryst.*, **198**, 465 (1991).

[25] Wilson, M.R., and Allen, M.P., *Liq. Cryst.*, **12** (1), 157 (1992).

[26] Huth, J., Mosell, T., Nicklaas, K., Sariban, A., and Brickmann, J., *J.Phys.Chem.*, **98**, 7685 (1994).

[27] Kroemer, G., Paschek, D., and Geiger. A., *Ber. Bunsenges. Phys. Chem.*, **97** (10), 1188 (1993).

[28] Cleaver, D.J., and Tildesly, D.J., *Mol. Phys.*, **81** (4), 781 (1994).

[29] Komolkin, A.V., Laaksonen, A., and Maliniak, A., *J. Chem. Phys.*, **101** (5), 4103 (1994).

[30] Frenkel, D., and Mulder, B.M., *Mol. Phys.*, **55**, 1171 (1985).

[31] Frenkel, D., Lekkerkerker, H.N.W., and Stroobants, A., *Nature*, **332**, 822 (1988).

[32] Frenkel, D., *Liq. Cryst.*, **5**, 929 (1989).

[33] Luckhurst, G.R., Stephens, R.A., and Phippen, R.W., *Liq. Cryst.*, **8**, 451 (1990).

[34] Luckhurst, G.R., *Ber Bunsenges. Phys. Chem.*, **97**, 1169 (1993).

[35] Nicklas, K , Bopp, P.A., and Brickmann, J. *Chem. Phys.*, **101** (4), 3157 (1994).

[36] Cross, C.W., and Fung, B.M., *J. Chem. Phys.*, **101** (8), 6839 (1994).

[37] Bhattancharjee, B., Paul, S., and Paul, R., *Mol. Cryst. Liq. Cryst.*, **89**, 181 (1982).

[38] Poon, C., Wooldbridge, C.M., and Fung, B.M., *Mol. Cryst. Liq. Cryst. Inc. Nonlin. Opt*., **157**, 303 (1988).

[39] Akasaka, K., Kimura, M., Naito, A., Kawahara, H., and Imanari, M., *J. Phys. Chem*., **99**, 9523 (1995).

[40] Sen, S., Brahama, P., Roy, S.K., Mukherjee, D.K., and Roy, S.B., *Mol. Cryst. Liq. Cryst.*, **100**, 327 (1996).

[41] Leadbetter, A.J., Temme, F.P., Heidemann, A., and Howells, W.S., *Chem. Phys. Lett.*, **34**, 363 (1975).

[42] Allen, M.P. and Tildesly, D.J., *Computer Simulation of Liquids*, Clarendon Press, Oxford (1990).

[43] Verlet, L., *Phys. Rev.*, **159**, 98 (1967).

[44] Gear, C.W., *Numerical Initial Value Problems in Ordinary Differential Equations*, Prentice-Hall, Englewood Cliffs, NJ (1971).

[45] Gear, C.W., Math. Compt., **21**, 146 (1967).

[46] Brooks, B.R., Bruccolerei, R.E., Olafson, B.D., States, D.J., Swaminathan, S., and Korplus, M., *J.Comp.Chem*., **4**, 187 (1983).

[47] Kast, S.M., Nicklas, K., Baer, H.-J., and Brickmann, J., *J.Chem.Phys*., **100**, 566 (1994).

[48] Berendsen, H.J.C., Postma, J.P.M., van Gunsteren, W.F., Di Nola, A., and Haak, J.R., *J.Chem.Phys*., **81**, 3684 (1984).

[49] Ciccotti, G., Ferrario, M., and Ryckaert, J.-P., *Mol. Phys*., **55**, 549 (1982).

[50] Ryckaert, J.-P., Ciccotti, G., and Berendsen, H.J.C., *J. Comput. Phys*., **23**, 327 (1977).

[51] Zannoni, C., In: *The Molecular Physics of Liquid Crystals* (Ed. G.R. Luckhurst, and G.W. Gray) ,Academic Press (1979).

[52] Tsvetkov, V., *Acta Physicochim*, **16**, 132 (1942).

[53] Eppenga, R., and Frenkel, D., *Molecular Physics*, **152** (6), 1303 (1984).

[54] Kast, S.M., and Brickmann, J., and Berry, R.S.,: The Interplay Between Quantum Chemistry and Molecular Dynamics Simulations. In: *Conceptual Perspectives in Quantum Chemistry* (Eds. J. Calais and E. Kryachko), pp. 195-223, Kluwer, Dordrecht, NL, (1997).

[55] Krueger, G.J., *Phys. Rep*., **82**, 229 (1982).

Hilfsmittel

Die Molekulardynamiksimulationen wurden mit Hilfe eines im Arbeitskreis vorhandenen Programms auf dem Hessischen Höchstleistungsrechner vpp300 in Darmstadt durchgeführt.
Teile der Auswertung und die Visualisierung wurden mit MOLCAD II, Plot und Transform erstellt. Der vorliegende Text wurde mit WORD97 geschrieben.

Curriculum Vitae

Name:	Saniye Pinar Sargin
Date of Birth:	23.02.1970
Place of birth:	Ankara

Schools:	1975-1980	Fevziatlioglu Primary School Ankara
	1980-1983	Kocatepe Mimar Kemal Secondary School Ankara
	1983-1986	Kocatepe Mimar Kemal High School Ankara
	1986-1987	Prepared School, Middle East Technical University (METU), Ankara
Undergraduate:	1987-1991	Bachelor of Science in Chemistry, METU Ankara
Graduate:	1991-1994	Master of Science in Chemistry, METU Ankara
	1991-1995	Research Assistant in Chemistry, METU Ankara
Dissertation:	1995-1999	Ph.D, in the working group of Prof. Dr. J. Brickmann, Institut für Physikalische Chemie I, TU Darmstadt

Eidesstattliche Erklärung

Hiermit erkläre ich an Eides Statt, daß ich meine Dissertation selbständig und nur mit den angegebenen Hilfsmitteln angefertigt habe.

Darmstadt, Dezember 1999